LUND UNIVERSITY

MASTER'S THESIS

DIVISION OF MATERIALS ENGINEERING

JANUARY 2016

WC grain size distribution during sintering of WC-Co cemented carbides

AUTHOR: OSCAR BJÄREBORN

SUPERVISORS: Dr. KUMAR BABU SURREDDI, LUND UNIVERSITY
Mr. TOMAS PERSSON and Ms. ANNA JOHANSSON, SECO TOOLS AB

EXAMINER: Professor SRINIVASAN IYENGAR, LUND UNIVERSITY

ISRN LUTFD2/TFMT--15/5052--SE

Preface

Special thanks to Professor Srinivasan Iyengar who introduced me to the interesting field of powder metallurgy. To Seco Tools AB who made this thesis possible; Tomas Persson and Anna Johansson who´ve supervised me there, set me straight when I've been confused and let me do my own project to the best of my abilities. Also thanks to all the other helpful people at Seco Tools AB for insightful discussions, to the guys in the production lab who performed the synthesis and all you who´ve showed me how things work. Also thanks to Dr. Kumar Babu Sureddi who agreed to take on the role as my supervisor at Lund University and continued to help me even after changing job.

Thanks to my partner Leticia for staying with me and supporting me even though I make her move around over the world.

This thesis has given me skills in analysis techniques and characterization, deepened my interest in powder metallurgy and given me insights in how research and industry works together.

Abstract

The grain growth of WC in WC-7%Co cemented carbides with Cr-addition was investigated for cemented carbides synthesized from four different raw materials varying in grain size. Cr additions were 4%of the Co binder phase. To investigate the effect of Cr on grain growth two of the raw materials were also synthesized without Cr-additions. To investigate the effect of cobalt content on grain growth cemented carbide with 13%Co with Cr addition was synthesized. All samples were sintered in four different cycles: 1300˚C for 10min, 1380˚C for 30min, 1430˚C for 1h and 1430˚C for 2h. Three of the samples were also sintered in a fifth sintering cycle at 1200˚C for 30min to investigate a sintering cycle with negligible grain growth for comparison with laser diffraction (LD) measurements of the WC powders, as milled. The evolution of the grain size distribution (GSD) for these sintering conditions were evaluated with electron backscatter diffraction (EBSD) measurements in a scanning electron microscope (SEM).

The grain growth observed during these sintering conditions is divided into three stages: A primary stage of rapid grain growth during solid state sintering with a prominent grain growth for the fine fraction, resulting in a narrowing of the GSD; A secondary stage of slower grain growth during liquid phase sintering; A tertiary stage where the large grains grow out of proportion to the rest of the population. The tertiary stage of grain growth was inhibited and the secondary was slowed down by Cr-additions, also the onset of densification in the initial stage was delayed with Cr-additions. Most likely, the delay of the initial stage is related to the presence of Cr- surface oxides which delay the spreading of Co at the beginning of densification. However, the delay of densification does not seem to have any significant effect on grain growth as sintering proceeds since Cr-additions lowers the melting temperature of Co. The inhibition at the secondary and tertiary stages is likely related to an inhibited precipitation of W and C atoms dissolved in the Co binder onto existing WC grains.

Variation in the critical misorientation angle for the determination of grains post EBSD-analysis is consistent with grain growth by coalescence in the early stage of grain growth. Also the dependences of hardness, fracture toughness and coercivity on grain size were evaluated. From these, correlations between coercivity and hardness/ fracture toughness were made which provides reasonable estimates of hardness and fracture toughness from coercivity for WC-7%Co with similar carbon content and Gaussian GSD.

Contents

Introduction and aim

Cemented carbides are interesting materials. Due to their high toughness/hardness ratio they have many applications and are widely used in the cutting tools industry. The cemented carbides combine the hardness of tungsten carbide (WC) crystallites with the toughness of a ductile binder phase. The most common binder phase being Cobalt (Co), chosen due to its excellent wetting ability of WC, which facilitates sintering. The WC crystallites form a hard skeleton submerged in a tough, shock-absorbent cobalt binder phase. However, the mechanical properties differ greatly with changes in composition and microstructure. The ability to tailor desired mechanical properties for specific applications is a powerful tool for the cemented carbide industry.

This thesis addresses some aspects of such tailoring with focus on the grain growth of tungsten carbide during different stages in the sintering. The grain size distribution is investigated as a whole, for different initial WC sizes and distributions as well as compositional changes. Correlations between changes in grain size and grain size distribution and mechanical properties such as hardness and fracture toughness are also investigated to facilitate tailoring of these properties. An evaluation of the ability to use non-destructive measurements of magnetic properties to estimate hardness and fracture toughness for the ranges in grain size distribution observed is also performed.

Theory

Synthesis

Cemented carbides are synthesized through a powder metallurgical route, where WC and Co particles are milled together with an organic binder and other additives. Homogenous slurry with water and ethanol is formed and subsequently spray dried into granules of identical composition. The powder consisting of about 100µm granules is then typically pressed into the desired shape. Thereby a “green body” is formed, which gets its mechanical strength from the organic binder. The green body is then heated to full density through liquid phase sintering.

The first step in the sintering cycle is to remove the organic binder which is done at 300-400˚C with the help of flowing hydrogen gas. Then follows a ramping up to 1250˚C in vacuum where oxides at the particle surfaces are reduced by carbon in the powder. There is typically some holding time of about 30 min at 1250˚C to even out the temperature profile in the sintering furnace before melting the binder phase. The actual liquid phase sintering with a peak temperature typically between 1380 and 1500˚C follows. There the Co melts and dissolves the smaller WC grains which then precipitate on the surface of larger WC grains, thus the grains grow. [1]

Carbon content

It is important to control the carbon content in the ternary W-C-Co system to stay in the desired two-phase structure of WC and Co binder. An excess of carbon will form a graphite phase upon cooling whilst insufficient amounts of carbon will lead to the formation of η-phase (primarily consisting of M_6C) upon cooling, see Figure 1. Both the appearance of graphite and in the η-phase is detrimental to the mechanical properties of the material.

For typical cooling rates used in industry it has been indicated that the dissolved tungsten in the binder, which is related to the carbon content, corresponds to the equilibrium value at approximately 1000˚C (see section on magnetization saturation below) [2, 3].

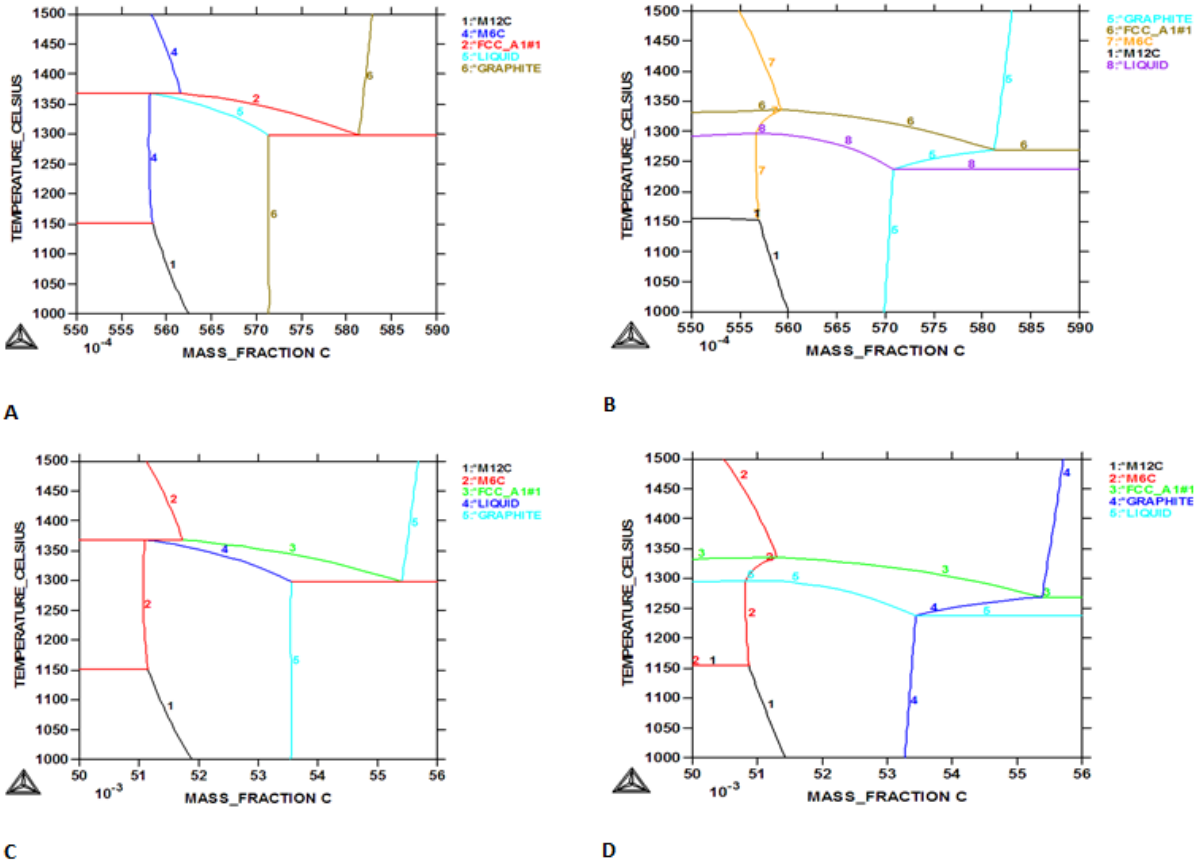

Figur 1, Phase diagram for: (A) W-C-Co with 7wt% Co, (B) W-C-Co-Cr with 7wt% Co and 0.28wt% Cr (i.e. Cr/Co=0.04), (C)W-C-Co with 13 wt% Co and (D) W-C-Co-Cr with 13wt% Co and 0.52wt% Cr (i.e. Cr/Co=0.04).

It has also been noted that the carbon content influences WC grain growth, where increased carbon content facilitates grain growth, as well as morphology, where increased carbon content gives more planar surfaces and triangular shapes [4].

Grain Growth

Tungsten carbide (WC) grains grow during sintering. Large grains grow at the expense of smaller grains. The WC crystallites (grains) can grow in two ways: amplification and multiplication. Amplification is the steady outward growth of a crystal by deposition of new atoms on its surface. Multiplication describes how grains merge as building blocks. Multiplication of grains is sometimes referred as coalescence, whilst amplification is the growth process that is driven by solution and precipitation.

Solution and precipitation

Smaller grains dissolve in the liquid cobalt binder phase more readily due to a higher surface energy and then precipitate on larger grains. In the WC-Co system the growth by amplification is regarded as being limited by the interfacial reactions occurring at the WC/WC and WC/Co boundaries, and not by diffusion as in the classical Ostwald ripening process. At a sharp solid/liquid interface two growth

modes are possible: 2D-nucleation and growth or defect assisted growth. For 2D- nucleation growth is limited by the creation of a nucleus on the otherwise flat surface. As the nucleus reaches a critical size, the growth parallel to the surface is comparatively fast, limited by diffusion of atoms to the advancing growth edge. For defect assisted growth defects at the solid/liquid interface (stacking faults or protruding dislocations) create growth sites [5], thus limited by the number of defects in the crystal.

Coalescence

Coalescence of adjacent crystals by aligning their orientations through slight rotations or translations is energetically favorable since it reduces the grain boundary energy of the system. Investigations have attributed an initial stage of rapid grain growth in the range of 1100-1300˚C, for powders ranging from 10-200nm in average size [6, 7] to the process of coalescence. As grain growth through coalescence does not require long range diffusion it is reasonable that it can occur at these relatively low temperatures.

Abnormal Growth

Coarsening of the WC grains in cemented carbide most often result in an asymmetric grain size distribution (GSD), where the larger grains account for the asymmetry as they grow larger than expected for a lognormal distribution. This can be seen as a tail in the representation of the GSD. The tail can be connected to abnormal grain growth, which occurs when a few grains grow more drastically at the expense of others [8]. This abnormal grain growth has been defined as “the case where the grain size distribution becomes wider than those predicted by the usual Oswald ripening theories” and the propensity for such growth increases with temperature and defects in the grains [9]. The abnormal grain growth becomes more significant for smaller grain sizes, showing a bimodal size distribution for submicron grains [10].

A model for grain growth has been proposed by Mannesson et al. [11] which is based on several processes: 2-D nucleation of growth ledges, mass transfer across the interface and long-range diffusion coupled in series. This model has showed good agreement with experimental results, for shorter sintering times, which is more applicable to practice [12]. Among other things it indicates the strong influence of the grain size distribution. However, it does not account for any of the many grain growth inhibitors used in the fabrication of cemented carbides.

Grain growth inhibition

The grain growth is strongly determined by the growth matrix, e.g. growth is strongly restricted in a Fe matrix, whereas strong growth occurs in a carbon rich Ni matrix. For WC-Co alloys the inhibition is determined by the nature and concentration of the additive related to the amount of binder, where V is the strongest inhibitor followed by Cr, Nb and Ta. The influence from the chemical nature of the binder phase on the WC grain growth can be seen as an interaction of the atoms involved in the growth process on the different stages of growth. Hence the influence of Fe or V on the growth can be seen as a strong interaction between C and Fe or V in the growth matrix forming very stable atomic clusters which builds a barrier against the nucleation of carbon in the growth process [10].

It has been found that when plotting hardness vs. toughness, for different grades of cemented carbides, grades with Cr additions are on the tougher side whilst V additions showed more scattered results. This indicates embrittlement at higher V to Co ratios [10]. For this thesis Cr will be the only

grain growth inhibitor investigated and toughness/hardness will be compared to straight WC-Co grades.

Analysis

Magnetic

For WC-Co cemented carbides the only ferromagnetic phase is the cobalt binder phase. The magnetic properties of the cemented carbide are useful in quality control where measurements are fast and non-destructive.

Magnetization saturation

The magnetization saturation is particularly useful in regards to verifying the carbon content of the cemented carbide. Magnetization saturation of the cobalt binder decreases with increasing amount of dissolved W [16] and can hence provide information on the amount of W dissolved in the binder phase. For typical cooling rates used in industry it has been indicated that the dissolved tungsten in the binder corresponds to the equilibrium value at approximately 1000˚C [2, 3]. The amount of carbon dissolved in the binder can then be estimated by applying the solubility product for WC.
It is convenient to normalize the saturation magnetization of a sample containing a certain amount of cobalt with the saturation magnetization of the same amount of pure cobalt; this ratio is called the relative saturation magnetization, denoted S. To stay within the two phase window and avoid the formation of either graphite- or η-phase empirical knowledge says that 0.75<S<0.98. There is also an empirical relationship for straight WC-Co grades between S and the overall carbon content in weight percent, %C, given by:

$$\frac{d\%C}{dS} \approx 0.074 \times \%Co$$

%Co is the overall cobalt content in weight percent [17]. However, the addition of Cr as a grain growth inhibitor lowers S without influencing the carbon content.

At Seco Tools the magnetization saturation is measured in the unit MM: equivalent to the percentage of W dissolved in the cobalt binder phase for straight WC-Co grades. For straight WC-Co grades 2<MM<14 corresponds to the two phase window, see Figure 1. It has been seen empirically that additions of Cr to the cobalt phase affects the magnetization saturation similarly to W dissolved in the cobalt and for every percent Cr added, below saturation, the two phase window is shifted one unit MM.

Coercivity

Coercivity measurements provide an indirect method for estimating grain size as the coercive force required to demagnetize cemented carbide is primarily related to the WC/Co interface area since the magnetic domain walls are pinned by these phase boundaries. The WC/Co interface area is inversely related to the WC grain size, which provides the basis for the grain size estimation. However coercivity is also affected by the composition of the Co binder phase, which may change with cooling rate and deformation (cold work). Also the WC/WC contiguity plays a role since two materials with similar grain size but different contiguity will have different interface areas, thus coercivity will differ. Contiguity is defined as the area fraction of grain boundaries that are WC/WC boundaries.

There are a number of empirical equations available in literature; however it is possible to derive a physically based model as described by B. Roebuck [18], on the following form:

$$H_C = a + \frac{b}{d_{WC}}$$

Where H_c is the coercivity, a and b are constants and d_{WC} is WC grain size as the arithmetic mean linear intercept obtained from a 2-D polished cross-section.

This model must however be considered a first approximation as it does not take into account the compositional effects on coercivity. Further it has been found from EBSD measurements, where the cross section area of each grain is used as a weight function, that the D10 value (defined as the equivalent diameter d_n where the area of grains smaller than d_n is equal to 10% of the total grain area) provides a better fit to this model than the D50 value (defined as the diameter d_n where the combined area of grains smaller and larger than this value are equal) [19]. This was observed for grain size distributions that had been deliberately skewed by mixing WC from different raw materials. It is reasonable that the D10 value be more closely related to the coercivity for such distributions as the smaller grains describe the distance between grains better for bimodal distributions. The model proposed by B. Roebuck [18] give a good fit to the grain size measured as the arithmetic mean linear intercept. It has however been shown that the importance of the fine fraction of grains is overestimated when using an arithmetic mean value [13].

Vickers Hardness and fracture toughness

Hardness

The Vickers Hardness indentation is applicable for hardmetals and cemented carbides, HV30 being advisable. Since hardmetals with HV30>1800 shows a high dependence of hardness on load it is advisable to use HV30 instead of e.g. HV10, also because the higher load lowers uncertainty, which is about ±100 for hardness values above 2000. However, uncertainties also depend on the magnification used for measuring the indentation [18].

Toughness

For indentation with a Vickers diamond indenter there is a simple relation between fracture toughness (K_{Ic}), the Palmqvist toughness (W) and the hardness (H) for WC-Co alloys, predicted by Shetty et al [20] as follows:

$$K_{Ic} = \beta\sqrt{HW}$$

Where β=0.089 for the standard Vickers indenter and

$$W = \frac{P}{4\bar{a}}$$

Where P is the load and $\bar{a}$ is the mean radial crack length.

Thus there is a convenient method for measuring fracture toughness in connection with the Vickers hardness, with reliable values for the fracture toughness when HV30 is above 1300 [21]. However the residual stresses which affect the crack lengths in the Palmqvist test are likely to be more significant

for the fine grained cemented carbides, and uncertainties are generally about ±1.5MNm$^{-3/2}$ for comparison between studies [18].

Hardness and grain size

The Hall-Petch relation in general predicts that the stress to deform to a given strain increases with decreasing grain size. Since the process of indentation results in plastic strain of at least 8% and plastic deformation of the WC phase occurs, it seems physically reasonable to model changes in hardness with changes in grain size [18]. The D50, as described above, has been found to give a good fit to such models [19], with the model on the following form:

$$H = a + \frac{b}{\sqrt{d_{WC}}}$$

Where H is the hardness, a & b are constants (for a given amount of Co binder), and d_{WC} is the WC grain diameter.

Scanning electron microscope – SEM

The SEM extracts electrons from the tip of an electron gun and accelerates them using a high tension, typically 2-30 kV, creating a beam of electrons. The electron beam is then focused with a set of magnetic lenses onto a spot on the sample, where various signals are generated as the electron beam interacts with the sample. The spot is scanned across the sample by varying the strength of magnetic coils. Simultaneously a detector, depending on the type of signal, records the intensity of the signal related to the location of the spot on the sample. By displaying the variations in intensity detected at the different places on the sample on a computer screen an image can be formed.

In SEM the electron beam is convergent and focused on a spot on the sample. At this spot a large amount of electrons are scattered incoherently and in all directions. Such electrons are sometimes referred to as diffusely scattered and these electrons can then be Bragg diffracted by the crystal planes. It is useful to think of the spot acting as a point source of electrons being scattered at all directions, some of them will be at an angle θ_{hkl} to the hkl planes in the crystal that fulfills the Bragg condition, being Bragg diffracted by these specific planes. Since the scattered electrons are travelling in all directions, the diffracted beam will lie on one of two cones, called Kossel cones. Thus we will see cones of diffracted electrons rather than well-defined beams, as we would in for example x-ray diffraction [22].

Electron Backscatter diffraction (EBSD)-detector

The EBSD-detector is a phosphor screen with a CCD- camera located at the side of the sample, which is tilted at 70°. As the scattered electrons hit the phosphor screen an image is recorded by the CCD-camera. There will be diffraction patterns associated with each spot which occur as lines (actually low angle parabolas) where the Kossel cones intersect the screen, called Kikuchi lines. The two Kikuchi lines make a band, through the center of which lies the geometric projection of the diffracting plane. The angular width of the band is twice the Bragg angle (θ_{hkl}). Hence the width of the band is related to the interplanar spacing d_{hkl} according to Bragg´s law:

$$2 * d_{hkl} \sin\theta_{hkl} = n * \lambda$$

Where n is the order of reflection, λ is the wavelength of the incident electron beam (related to the accelerating voltage of the SEM).

The extinction rules for expected reflections of the specific crystal structure are determined by the structure factor of the crystal. Since the geometry of Kikuchi diffraction patterns are unique for a particular crystal structure and crystal lattice orientation, it is possible to determine the grain orientation through indexing by measuring the position and width of some bands in the pattern [23].

The patterns are recorded with a stationary beam at a spot on the sample; the beam is then moved to the next spot where a new pattern is indexed. Thus an image can be created where the individual grains and their orientation can be identified.

Laser diffraction – LD

Laser diffraction is used for determining the particle size distribution on a volumetric basis (where the size of particles is calculated as that of a sphere of equivalent volume) by measuring how the particles scatter the light from a laser beam. The diffraction pattern is measured with intensity of scattered light as a function of angle. The diffraction pattern is related to the size of the particles. Large particles scatter light at low angles with rather high intensity, whereas smaller particles scatter light at larger angles but with lower intensity.

Upon measuring the diffraction pattern that arises as the sample scatters light, a first estimate of the particle size distribution is made. From the estimate a diffraction pattern can be calculated using Mie theory. The calculated diffraction pattern is then compared to the measured pattern. Alterations to the estimate of the size distributions are then made in an iterative manner to minimize the difference between the measured and calculated diffraction pattern.

The diffraction pattern is measured by a range of detectors at different angles and each detector has an angular range. The resulting size distribution is then represented with the relative frequency of particles in different size ranges, also called bins. These bins can be illustrated in a histogram or as cumulative frequency. The bins are however inherent of the measurement; laser diffraction does not measure individual particles but can calculate the size distribution [24].

Grain sizes

Some discrepancies are found considering what size measurements should be used to describe the grain size. The arithmetic mean linear intercept obtained from a 2-D polished cross-section has been widely used, although as described by H. Engqvist and B. Uhrenius [13] this method overestimates the influence of small grains significantly. It is reasonable to think that the influence of a grain on the macroscopic properties of the material is proportional to its volume (or mass). Since larger grains contribute to a larger volume in the bulk of the material. Thus including a weight function that represents the volume of the grain is appropriate. This could be done giving the distribution as a length fraction for the line intercept or an area fraction for area measurements of the grains. However a cross-section will always underestimate the actual value as it most likely does not cut through the largest part of the grain. A method to convert 2-D cross-section distribution into a 3D-distribution has been proposed by Jeppson et al. [14] and compared to 3D-EBSD measurements [15] where this model is in qualitative good agreement with the measured 3D-distribution. Jeppsson describes problems with the use of histograms, as their shape changes with the number of frequency bins used, and uses kernel estimators to correct for this. The 3D-distribution is then calculated and fitted to maintain the shape of the 2D-distribution.

A cumulative representation of the volume fraction of the grains would not have the problem as of the histogram as there is no binning involved. For adapting a 2D-distribution into 3D a calibration is proposed.

This calibration would be done with the distribution represented as the cumulative area fraction of a cross-section as measured with an EBSD-detector in a SEM, for a sample that has been sintered with negligible grain growth. This measurement would then be compared and calibrated with the distribution represented as the cumulative volume fraction of the WC powder in suspension as measured with laser diffraction and thereby give a reasonable conversion between 2D and 3D. However for empirical modelling the 2D-distribution is convenient, as it is readily obtained and results can be standardized.

All these measurement methods have the drawback of assuming a spherical grain, calculating the grain size as an equivalent circle (or sphere) diameter.

Experimental

Raw material

The grain growth of WC was investigated for four different raw materials, here denoted A, B1, B2 and C. Initial particle sizes as specified can be seen in Table 1. For A, B1 and C, agglomerates have been deagglomerated with light milling. B2 has been measured with agglomerated particles. For B1 and B2 specifications for coercivity are 9.4-10.3 kA/m after deagglomeration and sintering with 9 wt% Co at 1470˚C for 30 min with a carbon content corresponding to the middle of the two phase region. This indicates a similar grain size after such sintering conditions.

Table 1. A list of the raw material WC powders used with average grain sizes as per specification.

Raw material	Average particle size (µm)
A	0.82 ±0.03*
B1	2.3 ±0,3*
B2	5.8±0.2
C	3.6±0.3*

*deagglomerated

Composition

The composition of the cemented carbides produced was altered between 7 and 13 wt% Co binder phase. Additions of Cr were either 0 or 4 wt% of the binder phase. Carbon content was monitored through the magnetization saturation to be within the two phase window (see Figure 1). Carbon content was measured with magnetization saturation, and powders were modified to reach goal value, for samples sintered at 1430˚C for 1h, see section below. Any variations in carbon content for the other sintering cycles was not taken into account. The effect of variations in carbon content on the WC grain growth is considered to be outside the scope of this investigation. Compositions of the cemented carbides produced and analyzed can be seen in Table 2.

Table 2. Variations in composition for the investigated cemented carbides.

Cemented carbide (cc)	Raw Material	Co (wt%)	Cr (wt% of Co content)
1	A	7	4
2	A	13	4
3	B1	7	4
4	B1	7	0
5	B2	7	4
6	C	7	4
7	C	7	0

Sintering cycles

Initially four sintering cycles were used varying in top temperature and holding time to investigate the grain growth for the seven different cemented carbides. The top temperatures and holding times were: 1300˚C 10 min, 1380˚C 30 min, 1430˚C 1 h and 1430˚C 2h. However an additional sintering cycle with a top temperature of 1200˚C and a holding time of 30min was performed for cemented carbides (cc) 1, 6 and 7 to investigate if any significant grain growth had occurred before reaching 1300˚C.

Synthesis

4kg batches of powder were produced. Slurries were ball milled for 40h in slurry according to the specifications in Table 3 and subsequently spray dried. Some of the spray dried powder was separated for analysis with laser diffraction. Three standard square (SNUN120406, 15.4mm wide) bodies from each powder were pressed for each powder and sintering cycle in a hydraulic press at 171,6MPa. The pressed bodies were sintered in a vacuum sintering furnace according to the sintering cycles illustrated in Figure 2. For temperatures up to 450˚C hydrogen gas flowed through the furnace at approximately 20 slm to aid the degassing of the PEG. At the top temperatures of 1380˚C and 1430˚C Ar gas was flowed through the furnace at 3-5slm with 40mbar pressure to prevent the cemented carbide from sticking to the crucible, furnace specifications can be seen in Table 4.

Table 3. Milling parameters

Mill measurements	Ø192x200mm
Milling balls	12kg/mill (≈4g/ball)WC-Co
Milling liquid	0,8l ethanol (87%)
Rotational speed	44rpm
Lubricant/binder	2wt% PEG

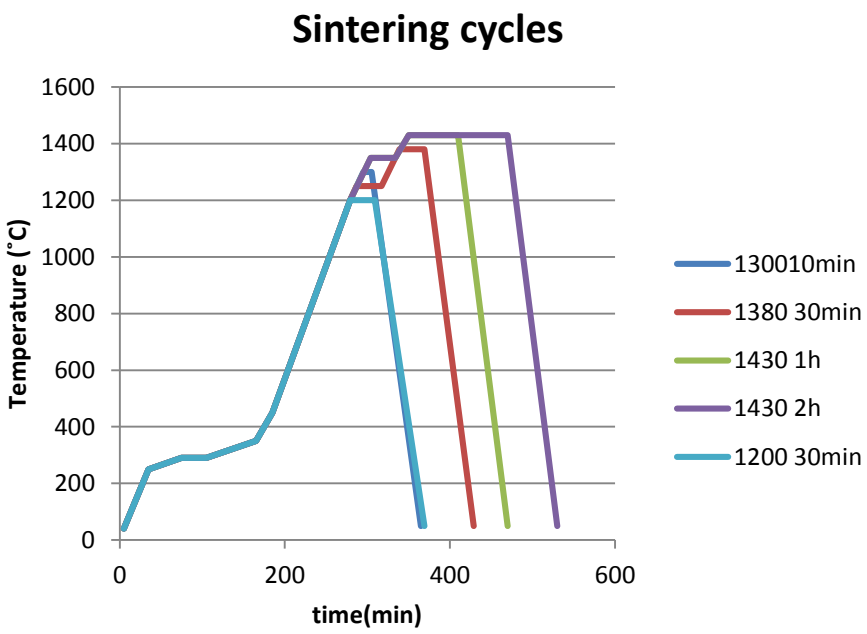

Figure 2. Sintering cycles with peak temperatures and holding times: 1200˚C 30min, 1300˚C 10min, 1380˚C 30min, 1430˚C 1h and 1430˚C 2h.

Table 4. Furnace specifications for COV231R

Max. Temperature	1600˚C
Tempeature tolerance	±10˚C
Work pressure	5*10^-3 < P< 1800 mbar
Min.Vacuum	8*10^-3 mbar
Gases	Ar, H_2,N_2,CO, CH_4

Sample preparation

For each powder one of the sintered bodies per sintering cycle were cut using a Struers Accutom 50 with a diamond blade. The cut surface was mechanically polished to 1µm using diamond slurries. For EBSD analysis the surface was further ion polished with 6,0keV Ar-ions for 4 hours in a Jeol SM-09010 cross section ion polisher at an incident angle of 1-2˚.

Analysis

Magnetic

Analysis of the magnetic properties was done before the cutting and polishing. Magnetization saturation and coercivity were measured with equipment from Förster-Koerzimat. Coercivity is given in kA/m and magnetization saturation was calculated to the unit MM: equivalent to the percentage of W in the cobalt binder phase for straight WC-Co grades. For straight WC-Co 2<MM<14 corresponds to the two phase window, see Figure 1. When adding chromium as a grain growth inhibitor the magnetization saturation decreases and 6<MM<18 corresponds to the two-phase window for grades with 4wt% Cr in the binder phase.

To control the carbon content magnetic saturation was measured for each of the 3 bodies sintered at 1430˚C for 1h, at least three times per body and an average value was calculated, uncertainties were about ±0.2MM. Coercivity was measured once per sintered body and uncertainties were about 0.05kA/m.

For straight WC-Co the goal value was MM=8 ±2 but when 4wt% Cr was added to the binder phase the goal value was instead MM=12±2. For bodies outside this range a new powder was produced until the goal value was achieved.

Hardness and toughness

Hardness measurements were made with a Future-Tech FV300 Vickers Hardness tester. Five indents 1mm apart with a 30kg load were made for each powder and sintering cycle, except for the porous bodies that resulted from the solid phase sintering cycles (1200˚C 30min and 1300˚C 10min) as the pores act as stress raisers and the hardness measured would be dependent on the pores instead of reflecting the properties of the cemented carbide. The sizes of the indentations were measured at 10 times magnification. Standard deviation never exceeded 28 HV30.

For the sintered bodies with HV30>1300 the toughness was calculated from the relationship by Shetty, see section above. Fracture toughness was calculated for each indentation and an average value was calculated for each specimen. The length of cracks (l) were measured from the corner of indentation at 1000 times magnification for cracks with l<100µm and at 500 times magnification for cracks with l>100µm in a Zeiss Axioplan light microscope. Standard deviations for the measurements of fracture toughness varied between 0.1 and 0.8 $MNm^{-3/2}$.

SEM- EBSD

The EBSD analysis was performed in a Zeiss Sigma VP scanning electron microscope equipped with an Oxford Instruments Nordlys EBSD-detector. A tension of 20kV, a 120µm aperture and a 16.0mm working distance was used for the analysis. The acquisition and evaluation of the EBSD data was performed with the Oxford Instruments Aztec and HKL Tango computer software programs. 4x4

binning and a gain of 5 were used. Solutions were found for 8 bands of the phases with the crystallographic data as described in Table 5.

Table 5. Crystallographic information of WC, Co (fcc) and Co (hcp) as provided by the CHANNELPhasedatabase in the Aztec software.

Phase	Space group	Cell parameters	Reflectors
WC	187	α=90˚, β=90˚,γ=120˚, a=b=2.91Å, c=2.84Å	41
Co (fcc)	225	α=β=γ=90˚, a=b=c=3.57Å	44
Co (hcp)	194	α=90˚, β=90˚,γ=120˚, a=b=2.51Å, c=4.07Å	41

Post processing and data cleaning was performed, with noise reduction and wild spikes filtering. Noise reduction changed pixels lacking of sufficient crystallographic information to the same as its neighboring pixels, level 5 was used, meaning it changes if more than 5 neighboring pixels have the same crystallographic information. Wild spikes filtering changes the information of lonesome pixels into that of their neighbors.

The step size was varied with the WC raw material used for each powder and held below 1/15 of the particle size as indicated by the supplier, see Table 1. About 800x600 pixels were analyzed per analysis and at least two analyses were performed per sample. Hit rates varied and were generally lower for samples with smaller grain sizes, although they were generally above 90% for the non-porous samples.

Initially the critical misorientation angle (CMA) used was 5˚. It was later changed to 1˚ to investigate if this affected the grain size distribution (GSD). Small changes in resulting GSD were observed for most samples using 1˚ CMA. However for cc- 6 and 7 (raw material C) significant changes were observed for sintering at 1200˚C 30min and 1300˚ 10min, especially for the fine fraction of grains. When the D10 value differed more than 3% between measurements using 1˚ and 5˚ CMA the GSD measured with 1˚ CMA was considered more accurate.

Grains the size of one and two pixels were removed from the data set. Incomplete grains at the frame of the analyzed window were not used. The total amount of grains analyzed, from all maps, per sample was never less than 8000 grains.

WC grains from EBSD measurements were plotted with the diameter as a function of the cumulative area fraction of the grains and the grain sizes were recorded as D10, D50, D90 and D95. The D10, D50, D90 and D95 values are defined as the equivalent diameter d_n where the area of grains smaller than d_n is equal to 10, 50, 90 and 95% respectively. Also an arithmetic mean size was calculated from the grains in each data set, called d_{mean}. The diameter of each grain was calculated as that of a circle with equivalent area.

Laser diffraction

For the laser diffraction analysis of the WC grain size, one powder per raw material was used, as neither the variations in cobalt content nor the small additions of chromium were thought to have any significant impact on the milling effect. About 1g of spray dried powder was treated with 40ml concentrated 5M hydrochloric acid to remove Cobalt and lubricant, first agitated with ultrasound and then left for 12h. The sample was then centrifuged at 3000 rpm for 30min and the clear supernatant was removed with a Pasteur pipette. 40ml deionized water was added to the sample which was then agitated with ultrasound and centrifuged again (at 3000rpm for 30min). The clear supernatant was removed again. The WC powder was then suspended in 40ml 1,5wt% coblock polymer-water solution. The particle size distribution was then analyzed with Malvern Mastersizer 2000, Laser diffractometer. Several measurements were performed and the result from those deemed good (i.e. with one peak in the expected size range) were averaged, ranging from 8 to 18 measurements per raw material. Measurements made with an additional peak of much larger particles than expected (≈100µm) were discarded and can be explained by the formation of bubbles.

For laser diffraction measurements the grain sizes are calculated as the diameter of a particle with equivalent volume. Grain sizes were recorded as D10, D50 and D90 defined as the equivalent diameter d_n where the volume of particles smaller than d_n is equal to 10, 50 and 90% respectively.

Results

Laser Diffraction (LD)

Table 6 shows the D10, D50 and D90 values for the different raw materials as measured with laser diffraction with standard deviation from the average values.

Table 6. D10, D50 and D90 values from laser diffraction measurements of WC after milling, shown as an average between measurements of the same powder (indicated uncertainties are standard deviations between measurements). The amount of measurements that contribute to the average value is also shown.

Raw material	D10 (µm)	D50 (µm)	D90 (µm)	Amount of measurements
A	0.25 ±0.01	0.59 ±0.02	1.11 ±0.04	9
B1	0,44 ±0.03	1.02 ±0.03	2.06 ±0.08	18
B2	0.54 ±0.06	1.4 ±0.11	2.9 ±0.24	8
C	0.52 ±0.02	1.47 ±0.05	3.0 ±0.1	14

Grain size distribution (GSD) from laser diffraction measurements of the WC grains after milling but before sintering can be seen in Figure 3 for each raw material. Figure 3 shows the WC grain size distributions for powders after milling. Horizontal error bars indicate the standard deviation of D10, D50 and D90 values. The GSDs shown in Figure 3 are averaged results of several measurements, see Table 6. It is notable that B2; which is specified as having a similar coercivity as B1 and thus grain size after milling and sintering with 9 wt% Co at 1470˚C for 30 min, has a more comparable GSD to C than to B1 at this stage. However measurements of B2 also have relatively high variations.

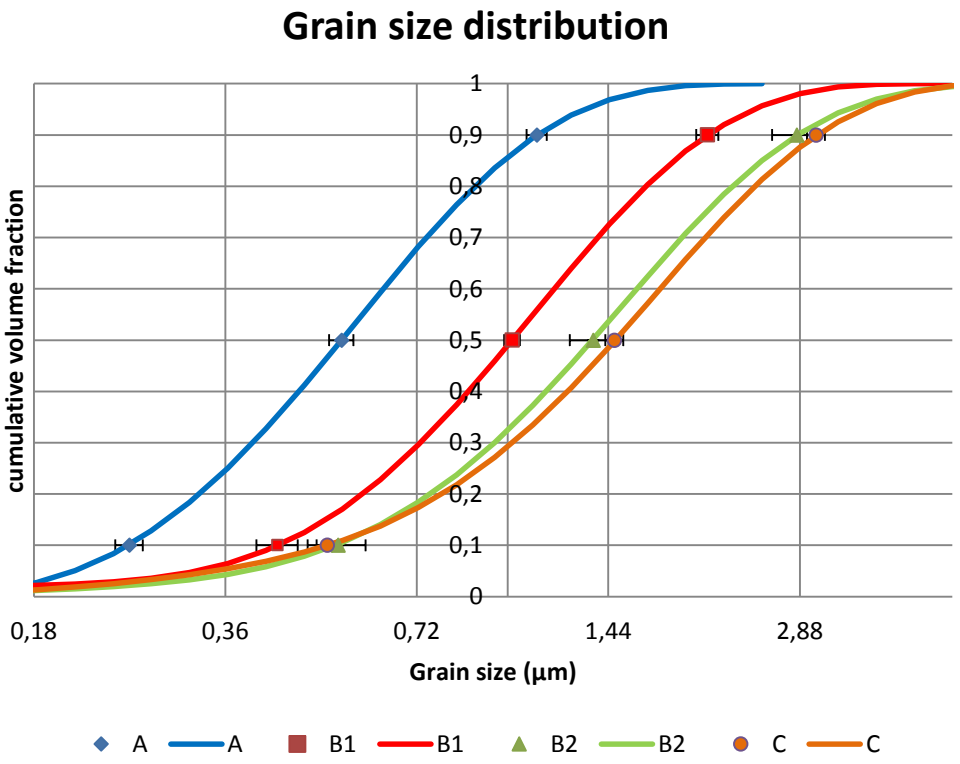

Figure 3, Grain size distributions for raw materials A, B1, B2, and C shown with the cumulative volume fraction as a function of grain size. Horizontal error bars show standard deviations for D10, D50 and D90 values averaged over several measurements

EBSD measurements

Examples of EBSD maps can be seen in Figure 4 and 5. Figure 4 shows a map of cc 1 (A 7Co 4cr) sintered at 1300˚C for 10min. From the large black areas of unidentified pixels in Figure 4 it is obvious that the cemented carbide is still porous at this stage. Figure 5 shows a map of cc 1 (A 7Co 4Cr) sintered at 1380˚C for 30min.

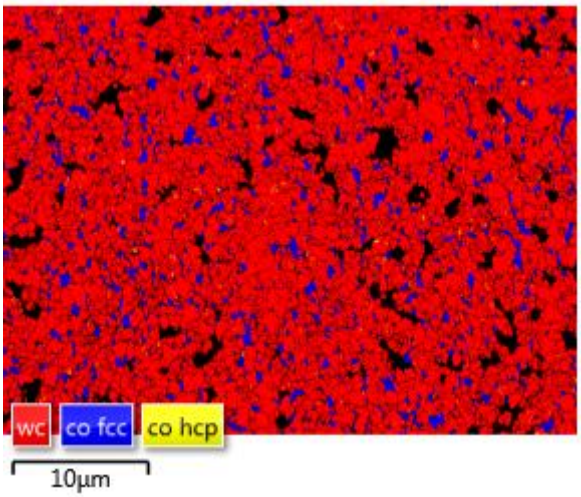

Figure 4, EBSD map of cc 1 (A 7Co 4Cr) sintered at 1300˚C for 10min with: WC (red), Co-fcc (blue), Co-hcp (yellow) and unidentified pixels (black).

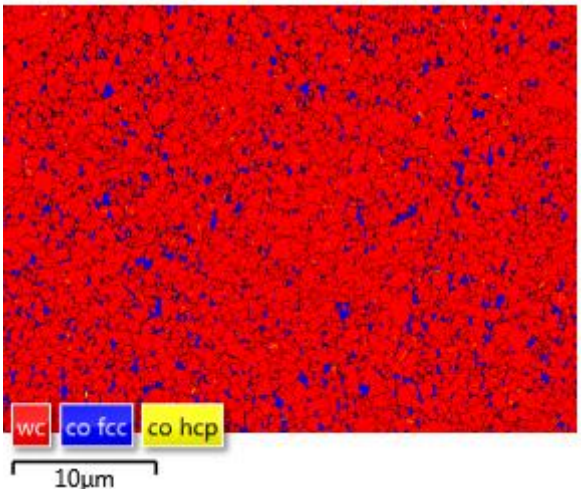

Figure 5, EBSD map of cc 1 (A 7Co 4Cr) sintered at 1380˚C for 30min with: WC (red), Co-fcc (blue), Co-hcp (yellow) and unidentified pixels (black).

Grain sizes measured as D10, D50 and D90, D95 and d_{mean} with EBSD for cemented carbides 1-7 sintered in different cycles can be seen in Table 7.

Table 7. Grain size as D10, D50, D90 and d_{mean} for cemented carbides 1-7 measured with EBSD at different sintering cycles.

Sintering cycle	Cemented carbide	D10 (µm)	D50 (µm)	D90 (µm)	D95 (µm)	d_{mean} (µm)
1200˚C 30min	1-A 7Co 4Cr	0.23	0.46	0.81	0.94	0.29
1300˚C 10min	1-A 7Co 4Cr	0.26	0.52	0.93	1.08	0.32
1380˚C 30min	1-A 7Co 4Cr	0.30	0.59	1.00	1.14	0.38
1430˚C 1h	1-A 7Co 4Cr	0.36	0.67	1.15	1.37	0.46
1430˚C 2h	1-A 7Co 4Cr	0.39	0.71	1.35	1.63	0.49
1300˚C 10min	2-A 13Co 4Cr	0.28	0.56	1.01	1.18	0.36
1380˚C 30min	2-A 13Co 4Cr	0.36	0.65	1.09	1.26	0.45
1430˚C 1h	2-A 13Co 4Cr	0.40	0.71	1.19	1.37	0.50
1430˚C 2h	2-A 13Co 4Cr	0.42	0.75	1.30	1.53	0.53
1300˚C 10min	3- B1 7Co 4Cr	0.52	1.07	1.89	2.17	0.49
1380˚C 30min	3- B1 7Co 4Cr	0.66	1.29	2.19	2.45	0.86
1430˚C 1h	3- B1 7Co 4Cr	0.72	1.32	2.31	2.81	0.91
1430˚C 2h	3- B1 7Co 4Cr	0.74	1.38	2.33	2.68	0.95
1300˚C 10min	4- B1 7Co 0Cr	0.55	1.14	2.03	2.36	0.70
1380˚C 30min	4- B1 7Co 0Cr	0.71	1.40	2.40	2.77	0.93
1430˚C 1h	4- B1 7Co 0Cr	0.79	1.46	2.59	2.95	1.00
1430˚C 2h	4- B1 7Co 0Cr	0.84	1.57	2.85	3.44	1.06
1300˚C 10min	5- B2 7Co 4Cr	0.61	1.31	2.33	2.66	0.75
1380˚C 30min	5- B2 7Co 4Cr	0.72	1.45	2.61	2.97	0.91
1430˚C 1h	5- B2 7Co 4Cr	0.82	1.61	2.80	3.23	1.05
1430˚C 2h	5- B2 7Co 4Cr	0.83	1.58	2.75	3.14	1.05
1200˚C 30min	6- C 7Co 4Cr	0.57	1.42	2.44	2.77	0.69
1300˚C 10min	6- C 7Co 4Cr	0.74	1.65	2.88	3.24	0.91
1380˚C 30min	6- C 7Co 4Cr	0.91	1.88	3.19	3.65	1.14
1430˚C 1h	6- C 7Co 4Cr	1.00	1.97	3.28	3.67	1.26
1430˚C 2h	6- C 7Co 4Cr	1.02	2.00	3.40	3.85	1.29
1200˚C 30min	7-C 7Co 0Cr	0.64	1.49	2.59	2.94	0.79
1300˚C 10min	7-C 7Co 0Cr	0.74	1.68	2.93	3.32	0.90
1380˚C 30min	7-C 7Co 0Cr	1.04	2.02	3.38	3.85	1.31
1430˚C 1h	7-C 7Co 0Cr	1.17	2.23	3.74	4.2	1.48
1430˚C 2h	7-C 7Co 0Cr	1.20	2.29	4.20	5.23	1.51

Comparison between LD and EBSD

Initial speculations of comparison between GSD measured on the powder before sintering with LD to GSD measured on sintered samples with EBSD for samples with supposedly negligible grain growth at 1300˚C for 10min were discarded. It was clear that grain growth had occurred at this stage from comparison with EBSD measurements for bodies sintered at 1200˚C for 30min, see Table 7. Comparison between LD-measurements and EBSD measurements for cemented carbides 1 and 6 sintered at 1200˚C for 30min can be seen in Figure 6. Figure 6 shows: the GSDs for raw material A and C obtained from LD measurements; GSDs for cemented carbides 1 and 6 sintered at 1200˚C for 30min; and conversion from 3D to 2D of the LD measurements. For the conversion between 3D and 2D in Figure 6 the grain sizes have simply been divided by a factor of 1.5 for comparison. This factor has been used empirically at Seco Tools AB. It is clear that the shapes of the GSDs differ and a steeper curve/more narrow distribution can be observed for sintered samples. It is also notable that the LD measurement (in 3D) for raw material C corresponds well with EBSD measurements of cc-6 (C 7Co 4Cr) sintered to 1200˚C for 30min for D50 values. Meanwhile grain sizes measured of raw material A by LD are relatively higher than what is seen for EBSD measurements of cc-1 at 1200˚C for 30min (A 7Co 4Cr).

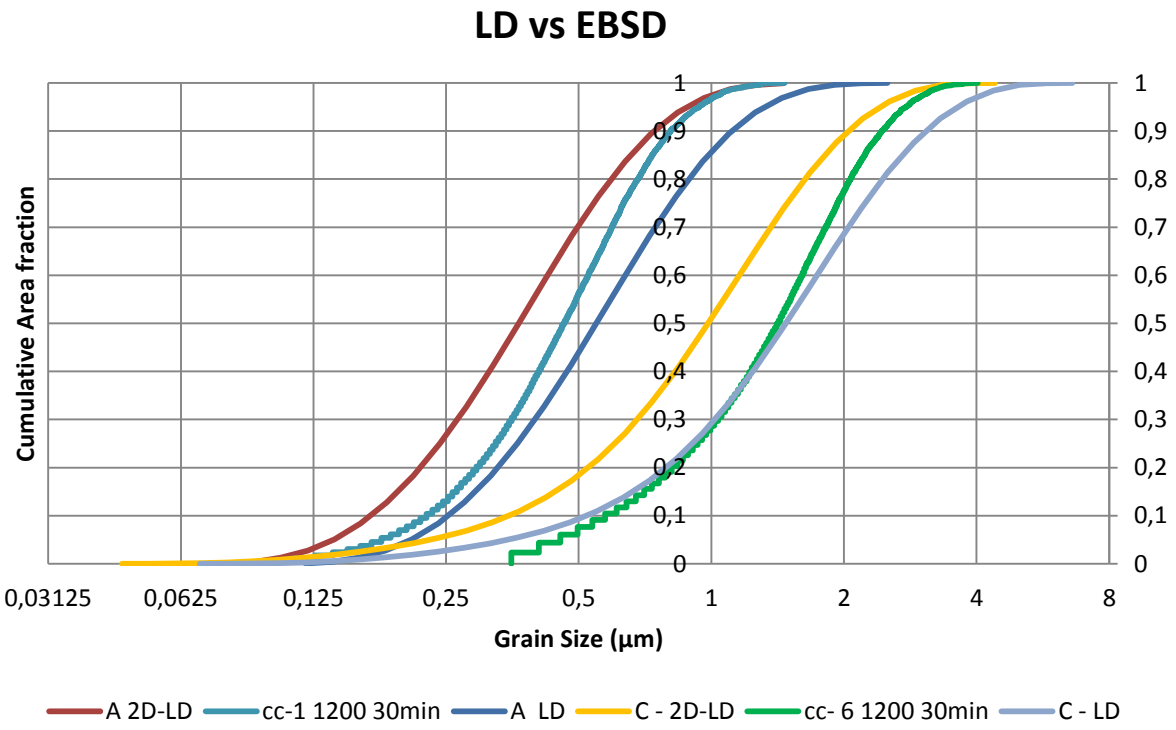

Figure 6. GSDs of raw materials A and C after milling obtained through LD measurements, GSDs of cemented carbides 1 and 6 (A 7Co 4Cr and C 7Co 4Cr) sintered at 1200˚C for 30min obtained through EBSD measurements and LD measurements converted to 2D for raw materials A and C.

Shrinkage/densification

For solid phase sintering (i.e. at 1200˚C for 30 min and 1300˚C for 10 min) the sintered bodies had not yet reached full density. The relative density reached where dependent both on the raw material used in the cemented carbide as well as the presence of Cr-additions. Cr-additions are found to decrease the densification in solid state sintered bodies. For cemented carbides with Cr-additions

those with larger WC grains reached lower densities when sintered to 1200˚C for 30min and 1300˚C for 10min.

Table 8 shows relative densities of cemented carbides 1-7 sintered at 1200˚ for 30min and 1300˚ 10min as well as the total linear shrinkage for samples sintered to full density. The relative densities are calculated from the width of the sintered bodies at solid state compared to the width at full density. Total shrinkage is calculated from the width at full density compared to the width of the green body (15.4mm).

Table 8. Width of solid sintered bodies, width at full density, relative density for solid sintered bodies and total shrinkage when full density is reached, for cemented carbides 1-7.

Cemented carbide	1200˚ 30min		1300˚ 10min		Full density	
	Width (mm)	Relative density %	Width (mm)	Relative density %	Width (mm)	Total shrinkage %
1- A 7Co 4Cr	14.3	89	13.2	97	12.8	16,8
2- A 13Co 4cr			13.2	97	12.8	16.8
3- B1 7Co 4Cr			13.1	97	12.7	17.5
4- B1 7Co 0Cr			13.0	98	12.7	17.5
5- B2 7Co4Cr			13.3	96	12.8	16.8
6- C 7Co 4Cr	14.9	84	13.6	94	12.8	16.8
7- C 7Co 0Cr	14.2	89	13.2	97	12.8	16.8

Grain growth

Independent variable -Sintering effect (K*min)

Since grain growth during sintering is dependent both on time and temperature an independent variable that is a function of both time and temperature has been used to demonstrate the effect of sintering parameters on grain growth. This variable, called sintering effect is calculated as the integral of temperature over time. Since the lowest sintering temperature used was 1200˚C and little can be said of what happens before 1200˚C, the GSD measured after sintering at 1200˚C for 30min is considered as the relative zero for grain growth and onset of the sintering effect is given as 1200˚C, according to:

$\int_{t=0}^{t}(T(t) - \mathbf{T(0)})dt$, Where T (0) =1200˚C

Hence the sintering effect is a physical representation of the area under the time-temperature curve above 1200˚C. The dependence of grain size on the sintering effect is displayed in Figure 7-10 for D10, D50, D90 and D95. In Figure 7-10 the horizontal error bars represent the error in sintering effect due to the 10K tolerance of the furnace and vertical error bars represent a 3% error in the measured grain sizes. 3% error is consistent with the difference allowed for D10 values when changing CMA between 5 and 1˚, as mentioned in the experimental section above.

The grain size for the fine fraction (D10) cemented carbides 1-7 as a function of sintering effect can be seen in Figure 7, where the grain growth is initially rapid and slows down for longer sintering cycles. Comparing cc-6 and 7, it can be noted that although they have similar D10 sizes initially cc-7 grows to a higher D10- size at a sintering effect of 10 000 (corresponding to sintering at 1380˚C for 30min), but then they grow at similar rates. A similar comparison can be made between cc-3 and 4, illustrating the effect of Cr-additions to the evolution of the fine fraction of grains. Comparing cc- 1 and 2 it is notable that cc-2 grows to slightly larger grain sizes for the fine fraction initially. However, the similar growth rates for cc-1 and 2 indicate that the effect of variations in cobalt content (between 7 and 13%) on grain growth is small for the fine fraction. Comparing cc-4 and 5 it is notable that the D10 value for cc-4 (B1 7Co 0Cr) reaches similar sizes as the D10 value for cc- 5 (B2 7Co 4Cr) when the sintering effect passes 10 000 K*min.

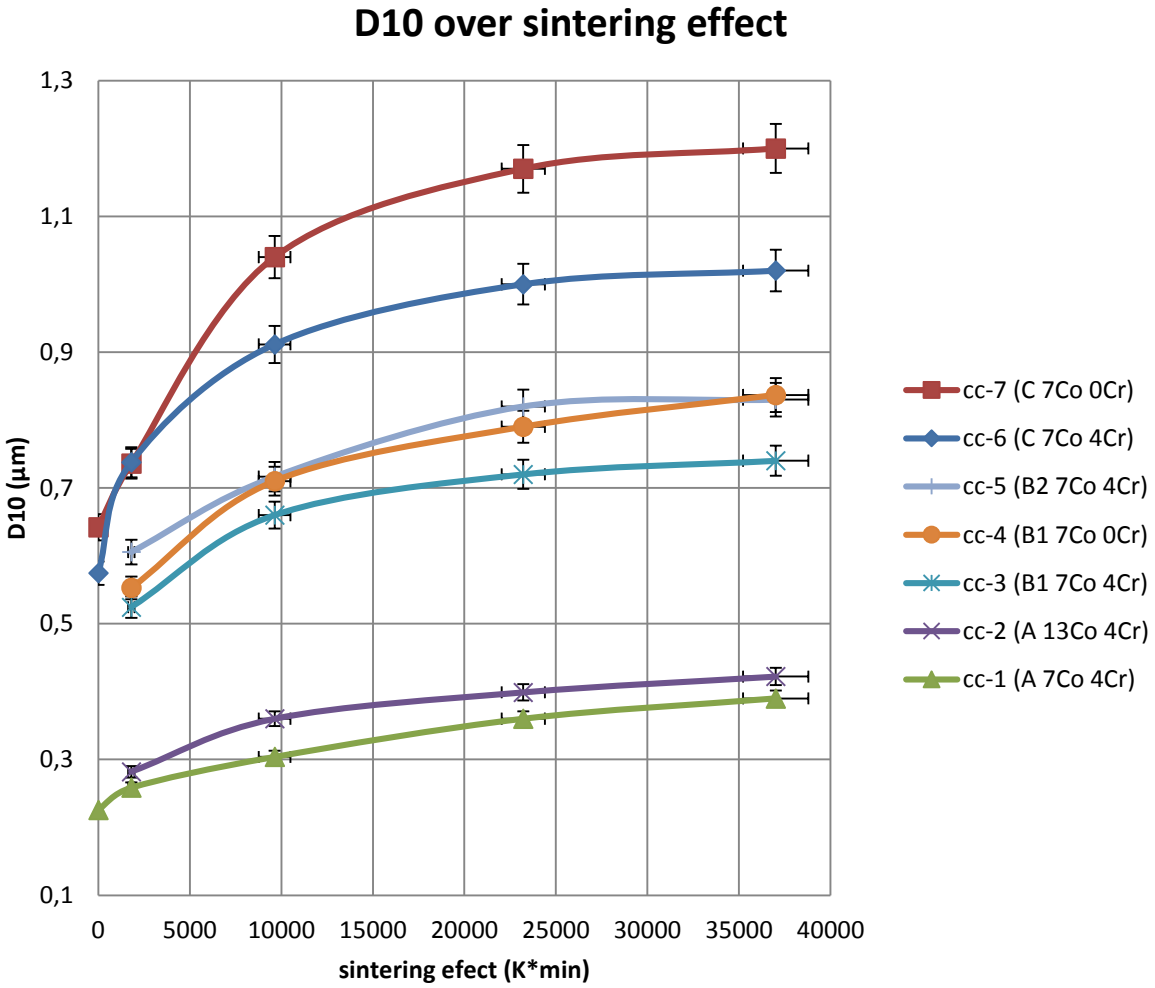

Figure 7, Grain size (D10) as a function of sintering effect for cemented carbides 1-7.

The grain size as D50 for cemented carbides 1-7 as a function of sintering effect can be seen in Figure 8. Figure 8 shows similar trends for the D50 value as shown for the D10 value in Figure 7. However comparisons between cc-6 and 7 and between cc- 3 and 4 for D50 shows a more continuous influence of Cr-additions to the D50 value as the sintering effect is increased, where the growth rate seems slightly higher for cemented carbides without Cr-additions throughout the sintering process. It is also noted that although cc-4 and 5 have similar D50 values after sintering to 1380˚C for 30min and to 1430˚C for 2h, their D50 values differ after sintering to 1430˚C for 1h. Further D50 for cc- 1 and 2 show only small differences, where the D50 for cc- 2 is slightly larger than the D50 for cc- 1.

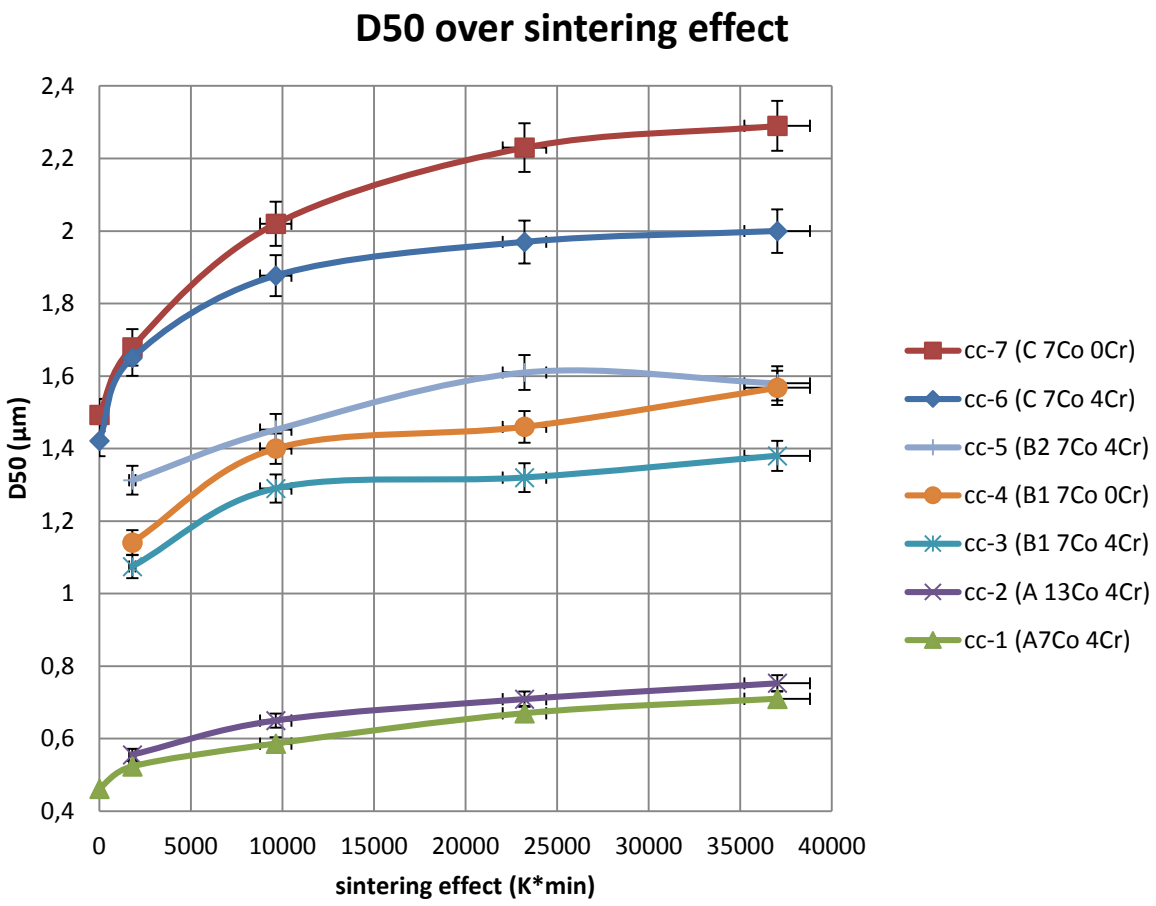

Figure 8, Grain size (D50) as a function of sintering effect for cemented carbides 1-7

The grain size as D90 for cemented carbides 1-7 can be seen in as a function of sintering effect in Figure 9. Figure 9 shows similar trends for the D90 value as shown for the D10 and D50 values in Figure 7 and 8 for cemented carbides with Cr-additions. However Figure 9 shows a much higher growth rate of D90 for cc- 7 and 4 (no Cr) at the later stages of sintering. It is notable that the D90 value for cc- 4 is significantly lower than the D90 value for cc-5 for all sintering cycles but the last one (1430˚C 2h), where the D90 value of cc-4 surpasses the D90 value for cc-5. Also the D90 value for cc-1 surpasses the D90 value for cc-2 after sintering to 1430˚C for 2h.

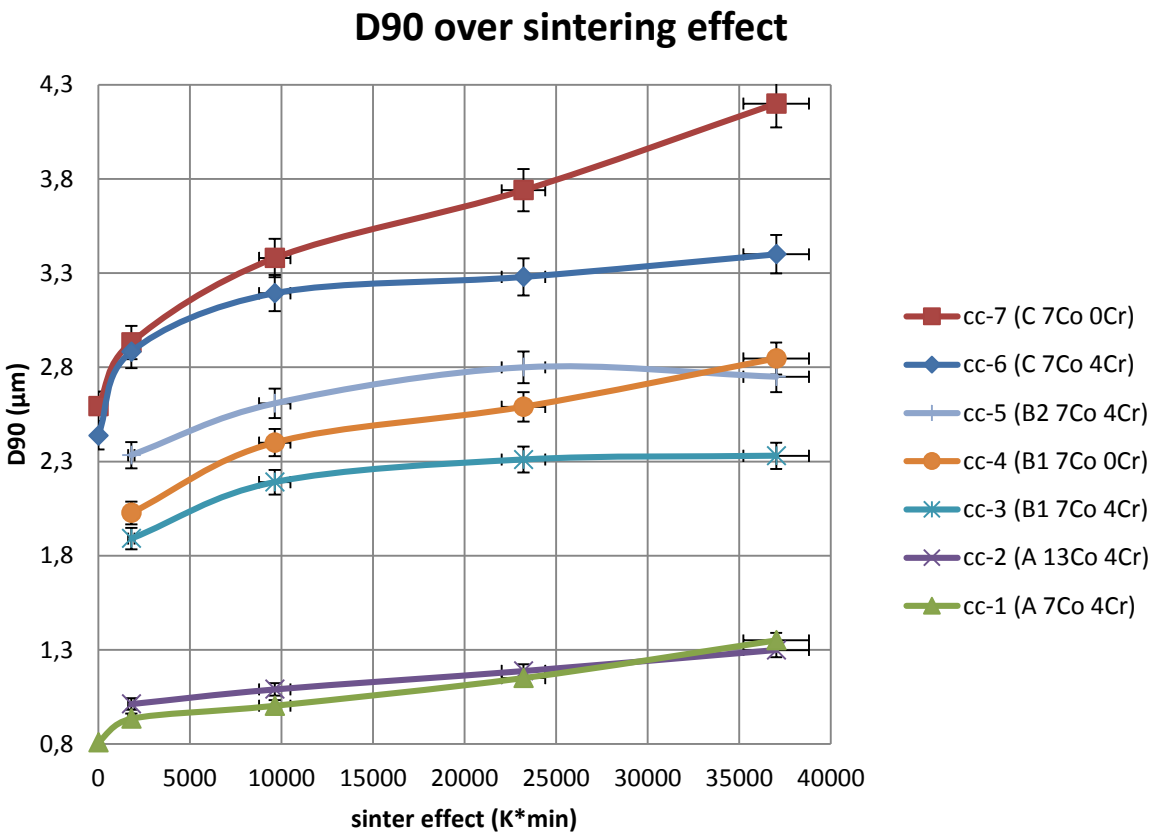

Figure 9, Grain size (D90) as a function of sintering effect for cemented carbides 1-7.

The grain size as D95 for cemented carbides 1-7 can be seen as a function of sintering effect in Figure 10. Figure 10 shows similar trends for the D95 value as shown for the D90 value in Figure 9. However Figure 10 shows a more marked increase in the growth rate for the D95 value for cc- 7 and 4 (no Cr) than could be seen for the D90 value in Figure 9. It is also noted that the D95 value for cc-1 surpasses the D95 value for cc-2 after sintering to 1430˚C for 2h, as could be seen for the D90 value in Figure 9. An oddity observed in Figure 10 is that the D95 value for both cc- 3 and 5 seem to decrease between sintering to 1430˚C for 1h and 1430˚C for 2h.

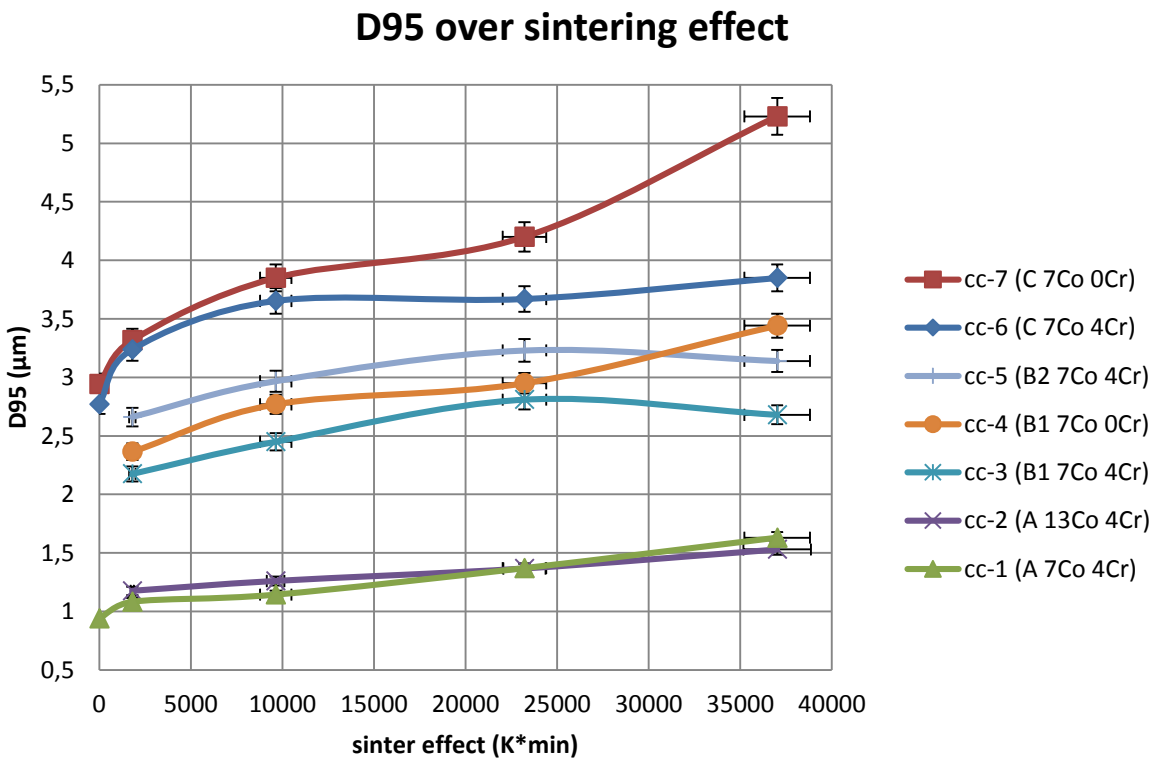

Figure 10, Grain size (D95) as a function of sintering effect for cemented carbides 1-7

.

Variations in critical misorientation angle - CMA

Variations in CMA between 1 and 5˚ resulted in small variation in the GSD measured by EBSD for some cemented carbides where a smaller fine fraction was consistently measured when using 1˚. The increase observed in the D10 value measured going from 1 to 5˚ can be seen in Table 9. The variations observed in the GSD were found to decrease with initial particle size and gradually disappear for later sintering stages. Cemented carbides with Cr-additions displayed larger such variations and the largest variations was found for cc-6 (C 7Co 4Cr), see Figure 11. Figure 11 shows how the GSD varies when defining the grains with a CMA of 1 or 5˚ for cemented carbide 6, sintered

at 1200˚C for 30min, 1300˚C 10min and 1380˚C for 30min. Variations decrease as the sintering process goes along.

Table 9. Increase in D10 between measurements made with 1 and 5˚ CMA.

Sintering cycle	cc-1 (A 7Co 4Cr)	cc-2 (A 7Co 4Cr)	cc-3 (B1 7Co 4Cr)	cc-4 (B1 7Co 0Cr)	cc-5 (B2 7Co 4Cr)	cc-6 (C 7Co 4Cr)	cc-7 (C 7Co 0Cr)
1200˚C 30min	6%	-	6%	4%	5%	27%	18%
1300˚C 10min	3%	-	-	-	5%	10%	10%
1380˚C 30min	-	-	-	-	-	3%	-

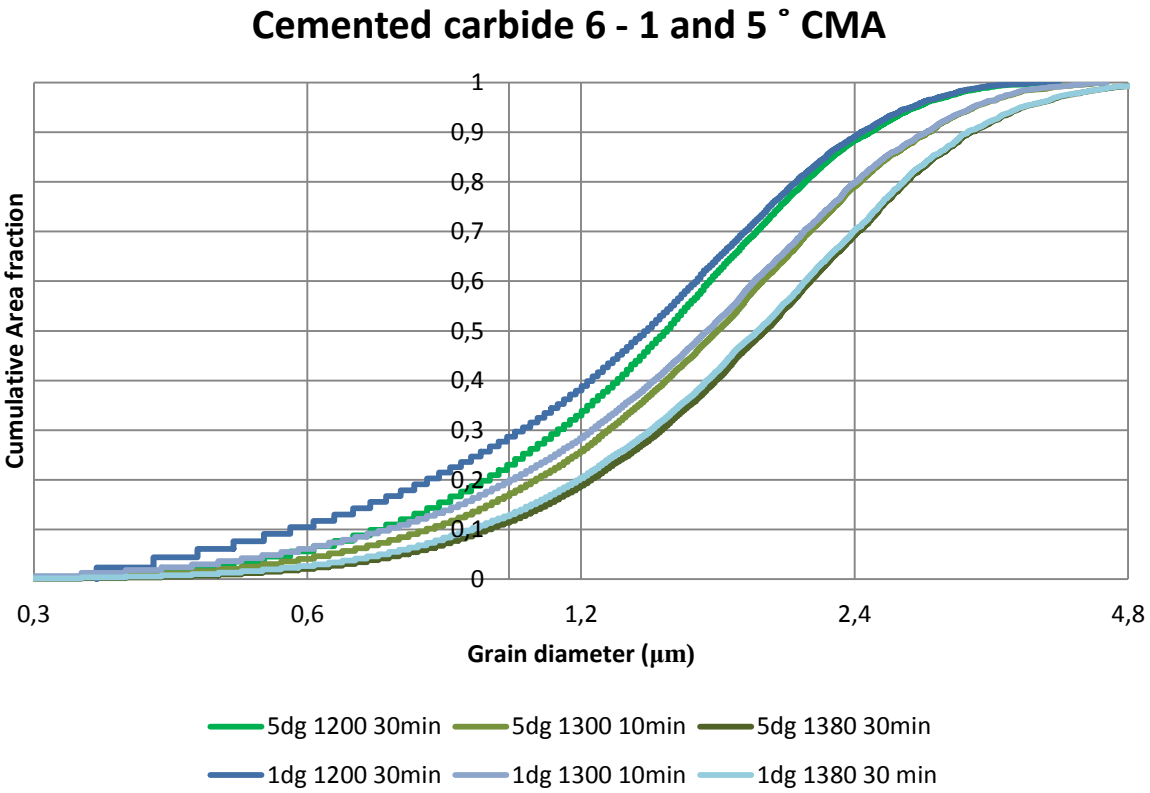

Figure 11, Cumulative area fraction of grains measured by EBSD as a function of grain diameter for cc-6 at 1200˚C 30 min, 1300˚C 10min and 1380˚C 30min, grains defined with a CMA of 1 and 5˚.

Mechanical and magnetic properties

Table 10 shows the magnetization saturation (Ms), coercivity (Hc), hardness (HV30), fracture toughness (K_{1C}) and D50 value measured by EBSD, for the cemented carbides 1-7 after sintering in the different cycles. Uncertainties for hardness and fracture toughness are indicated with the standard deviations.

Table 10. Magnetization saturation (Ms), Coercivity (Hc), Hardness (HV30), fracture toughness (K_{1C}) and grain size as D50 for cemented carbides 1-7. Hardness and toughness values are given as an average over 5 measurements, uncertainties indicate the standard deviation.

Sintering cycle	Cemented carbide	Ms (MM)	Hc (kA/m)	HV30	K_{1C} (MN/m^{1,5})	D50 (µm)
1200˚C 30min	1-A 7Co 4Cr	11.5	25,3	-	-	0.46
1300˚C 10min	1-A 7Co 4Cr	11.7	22.3	-	-	0.52
1380˚C 30min	1-A 7Co 4Cr	12.3	24.8	1736±3	9.4±0.1	0.59
1430˚C 1h	1-A 7Co 4Cr	12.0	23.2	1719±6	9.6±0.1	0.67
1430˚C 2h	1-A 7Co 4Cr	12.3	22.4	1689±8	8.9±0.2	0.71
1300˚C 10min	2-A 13Co 4Cr	12.2	16.1	-	-	0.56
1380˚C 30min	2-A 13Co 4Cr	12.4	17.9	1438±4	13±0.4	0.65
1430˚C 1h	2-A 13Co 4Cr	12.3	17.0	1427±6	12.7±0.2	0.71
1430˚C 2h	2-A 13Co 4Cr	12.8	16.7	1420±10	12.9±0.3	0.75
1300˚C 10min	3- B1 7Co 4Cr	10.4	14.6	-	-	1.07
1380˚C 30min	3- B1 7Co 4Cr	10.7	15.1	1517±3	11.1±0.2	1.29
1430˚C 1h	3- B1 7Co 4Cr	10.5	14.8	1520±10	10.6±0.1	1.32
1430˚C 2h	3- B1 7Co 4Cr	10.8	14.7	1522±5	10.8±0.2	1.38
1300˚C 10min	4- B1 7Co 0Cr	5.2	13.3	-	-	1.14
1380˚C 30min	4- B1 7Co 0Cr	5.4	13.2	1456±6	11.2±0.3	1.40
1430˚C 1h	4- B1 7Co 0Cr	6.2	12.8	1447±5	11.3±0.2	1.46
1430˚C 2h	4- B1 7Co 0Cr	6.3	12.7	1435±9	11.5±0.2	1.57
1300˚C 10min	5- B2 7Co 4Cr	11.9	13.8	-	-	1.31
1380˚C 30min	5- B2 7Co 4Cr	11.9	13.9	1479 ±7	12.0±0.3	1.45
1430˚C 1h	5- B2 7Co 4Cr	11.9	13.6	1480±24	11.4±0.2	1.61
1430˚C 2h	5- B2 7Co 4Cr	12.1	13.4	1472 ±3	11.5±0.2	1.58
1200˚C 30min	6- C 7Co 4Cr	14.1	15.1	-	-	1.42
1300˚C 10min	6- C 7Co 4Cr	14.1	12.4	-	-	1.65
1380˚C 30min	6- C 7Co 4Cr	14.3	12.0	1400±28	12.0±0.2	1.88
1430˚C 1h	6- C 7Co 4Cr	14.2	11.7	1390±7	12.8 ±0.1	1.97
1430˚C 2h	6- C 7Co 4Cr	13.9	11.6	1388±6	13.4±0.3	2.00
1200˚C 30min	7-C 7Co 0Cr	8.4	11.8	-	-	1.49
1300˚C 10min	7-C 7Co 0Cr	8.5	11.0	-	-	1.68
1380˚C 30min	7-C 7Co 0Cr	8.8	11.0	1363±4	12.8±0.3	2.02
1430˚C 1h	7-C 7Co 0Cr	9.2	10.3	1357±7	14.0±0.8	2.23
1430˚C 2h	7-C 7Co 0Cr	9.4	10.1	1347±6	13.7±0.6	2.29

Hardness vs. WC grain size

A linear relation was made between the hardness and $\frac{1}{\sqrt{Grain\ size}}$, using D10, D50, D90 and d_{mean} (the arithmetic mean grain size) for cemented carbides with 7%Co according to the Hall- Petch relation, see Figure 12.

Values of R^2>0.95 were obtained for all four trend lines, with the highest value for D50 measurements with R^2=0.966.

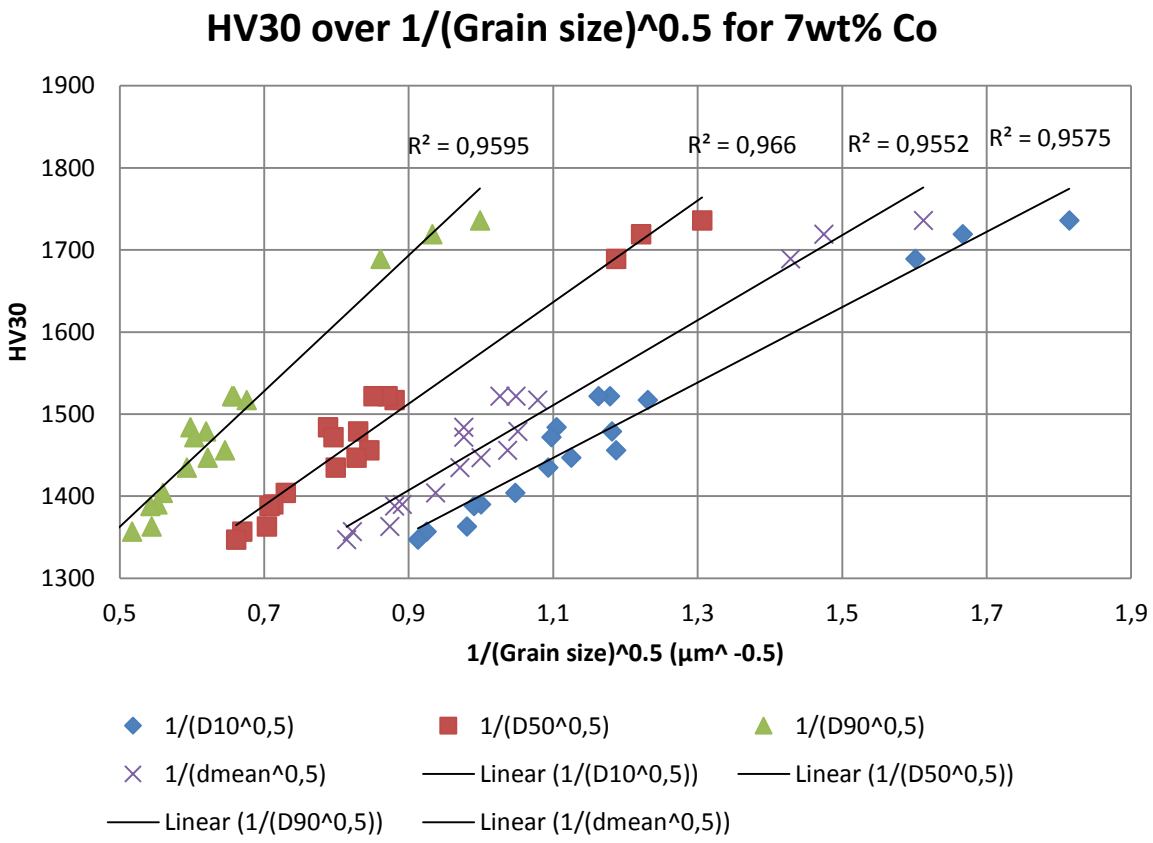

Figure 12, Hardness plotted against 1 over the square root of grain size measured as D10, D50, D90 and dmean with linear trend lines and coefficients of determination (R^2) displayed for each data set, for cemented carbides with 7% Co.

Figure 13 shows the dependence of hardness to the inverse square root of grain size measured as D50 for 7%Co 4Cr, 7%Co 0Cr and 13%Co 4Cr. The hardness relation to grain size differs significantly as the amount of Co binder changes between 7 and 13%. A minor difference is observed between 0 and 4% Cr in the Co binder. With the Cr doped samples being slightly harder.

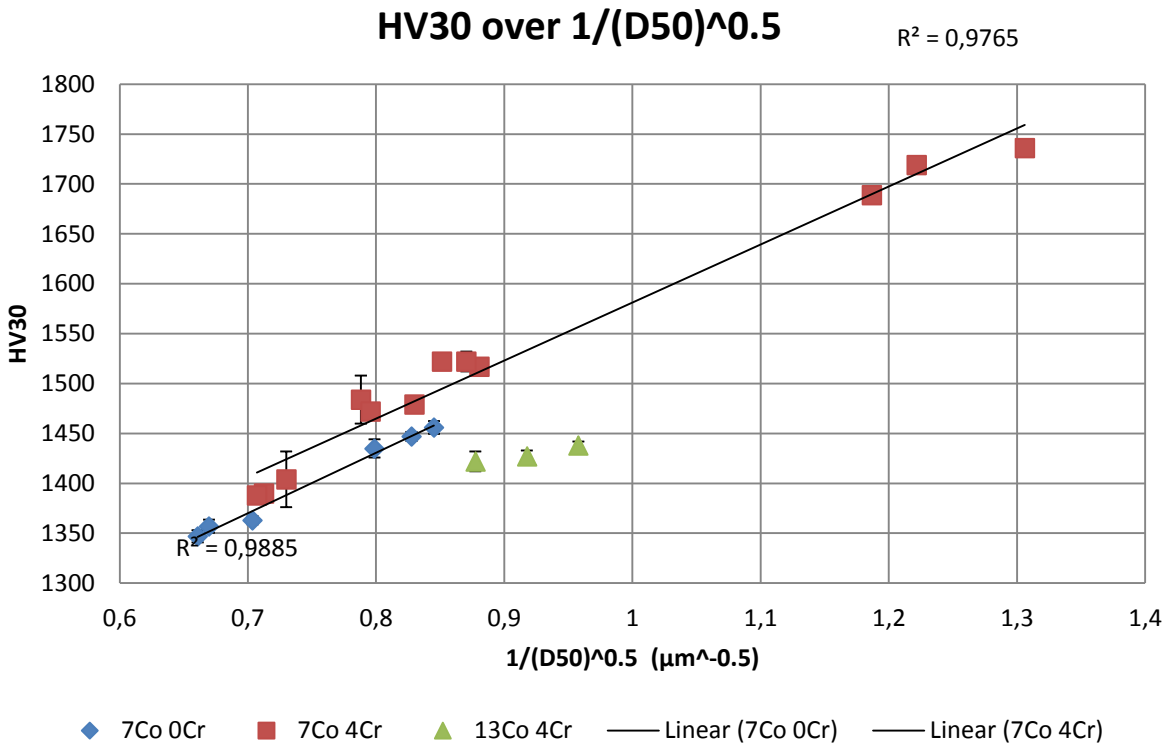

Figure 13. Hardness plotted against 1 over the square root of grain size measured D50 for cemented carbides with: 7%Co 4%Cr (red), 7%Co 0%Ct (blue) and 13%Co 4%Cr (green) with linear trend lines and coefficients of determination (R^2) displayed for cemented carbides with 7% Co

Coercivity vs WC grain size

A linear relation was made between the coercivity (Hc) and $\frac{1}{Grain\ size}$, using D10, D50, D90 and dmean (the arithmetic mean grain size) for cemented carbides with 7%Co that had been liquid phase sintered (i.e. at 1380˚C for 30min, 1430˚C for 1h and at 1430˚C for 2h), see Figure 14 . The D50 value gave the better fit for such a linear relation. Coercivity for cemented carbides with 13%Co as well as the coercivity for samples that had been solid state sintered (i.e. at 1200˚C for 30min and 1300˚C for 10min) deviates from this linear relation as seen in Figure 15.

Figure 14 shows the dependence of coercivity (Hc) on the reciprocal grain size for cemented carbides with 7%Co sintered to liquid phase, measured as D10, D50, D90 and dmean. Linear trend lines and coefficients of determination (R^2) are displayed for each data set. Values of R^2>0.97 were obtained for all four trend lines, with the highest value for D50 measurements with R^2=0.987 All four linear trend lines intercept the y-axis at 5.5 ±0.1 kA/m.

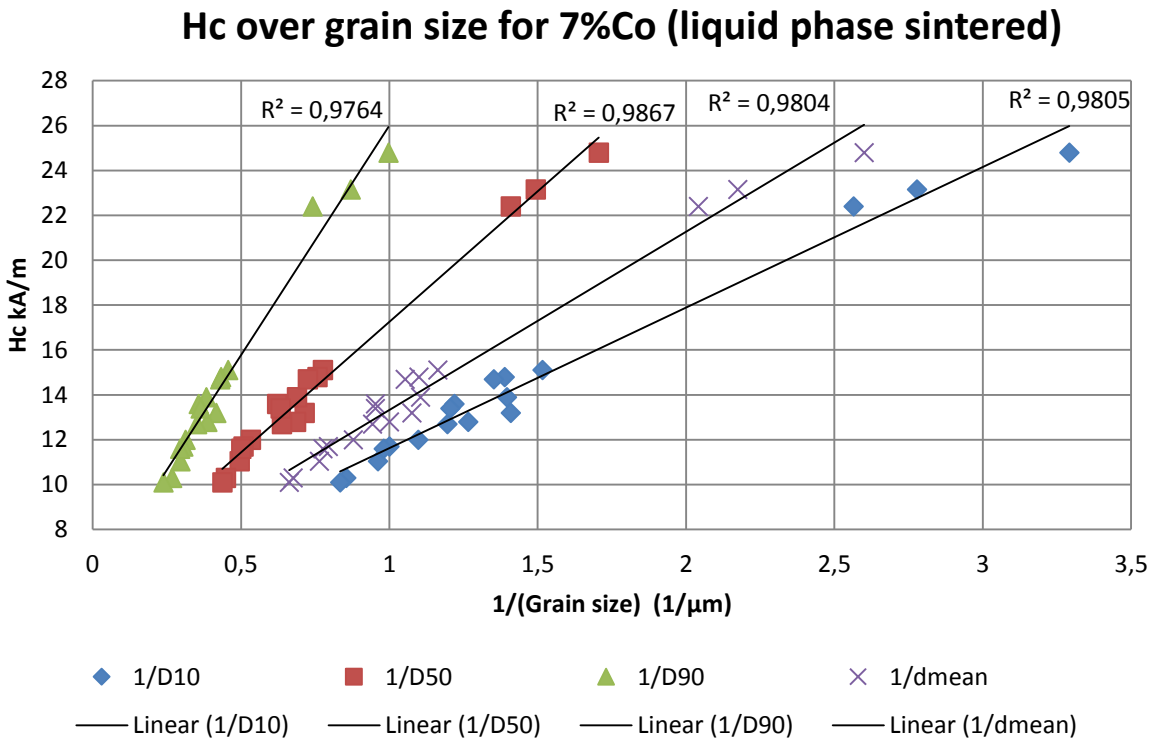

Figure 14, Coercivity plotted against the inverse grain size measured as D10, D50, D90 and dmean with linear trend lines and coefficients of determination (R^2) displayed for each data set, for cemented carbides with 7% Co sintered at 1380˚C for 30min, 1430˚C for 1h and at 1430˚C for 2h.

Figure 15 shows the dependence of coercivity with reciprocal grain size, measured as D50, for cemented carbides with 7%Co 4Cr, 7%Co 0Cr and 13%Co 4Cr. Bodies sintered at liquid phase (1380˚C for 30min, 1430˚C for 1 h and 1430˚C for 2h) and in solid state (1200˚C for 30min and 1300˚C for 10min) are indicated separately. Coercivity deviates for cemented carbides with 13%Co, where lower coercivity is observed for similar grain sizes. Coercivity for cemented carbides sintered in solid state deviate from the coercivity observed when liquid phase sintered, exhibiting lower coercivity than expected from the linear trend seen in Figure14. Cemented carbides with smaller grain sizes show larger deviations from the linear trend.

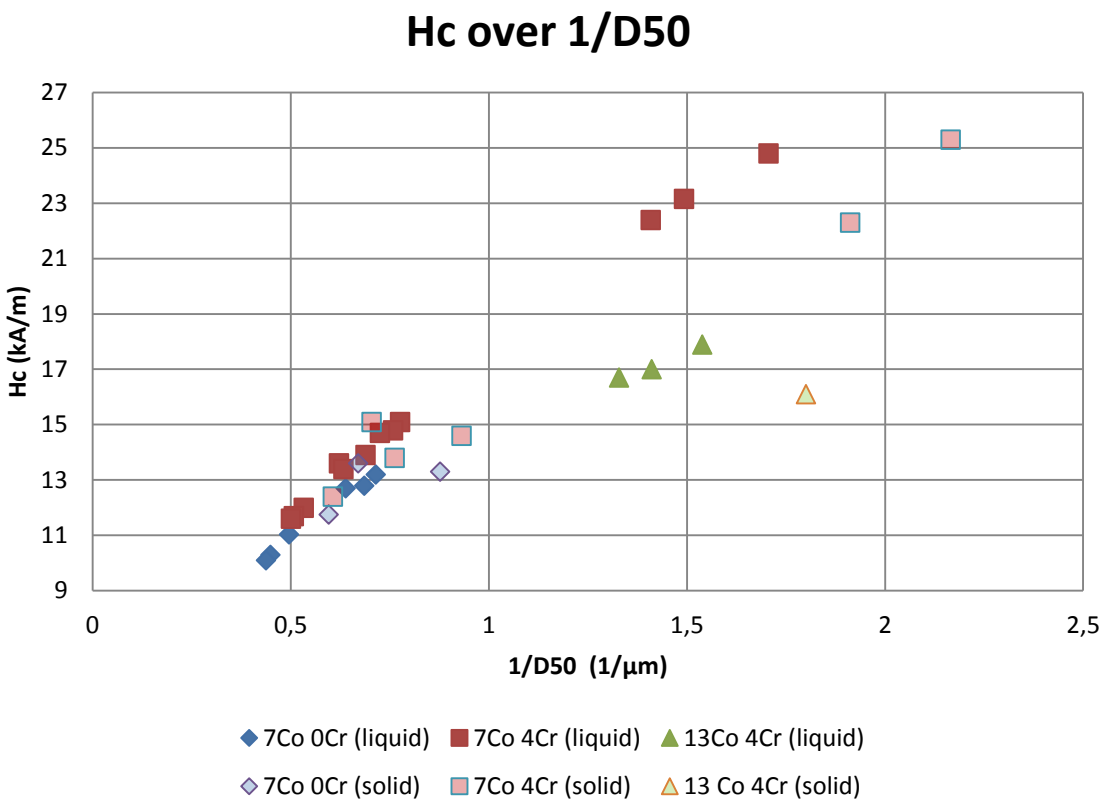

Figur 15, Coercivity plotted against the inverse grain size measured as D50 for cemented carbides with 7%Co and 4%Cr (red), 7%Co and 0%Cr (blue) and 13%Co and 4%Cr (green) for bodies sintered in liquid phase (solid marker fill) and solid state sintered (transparent marker fill).

Toughness vs. size

A linear relationship between the fracture toughness (K_{1C}) and the grain size for cemented carbides with 7%-cobalt was found using the D10, D50, D90 and dmean values, see Figure 16.Values of R^2>0.91 were obtained for all four trend lines, with the highest value for D50 measurements with R^2=0.934.

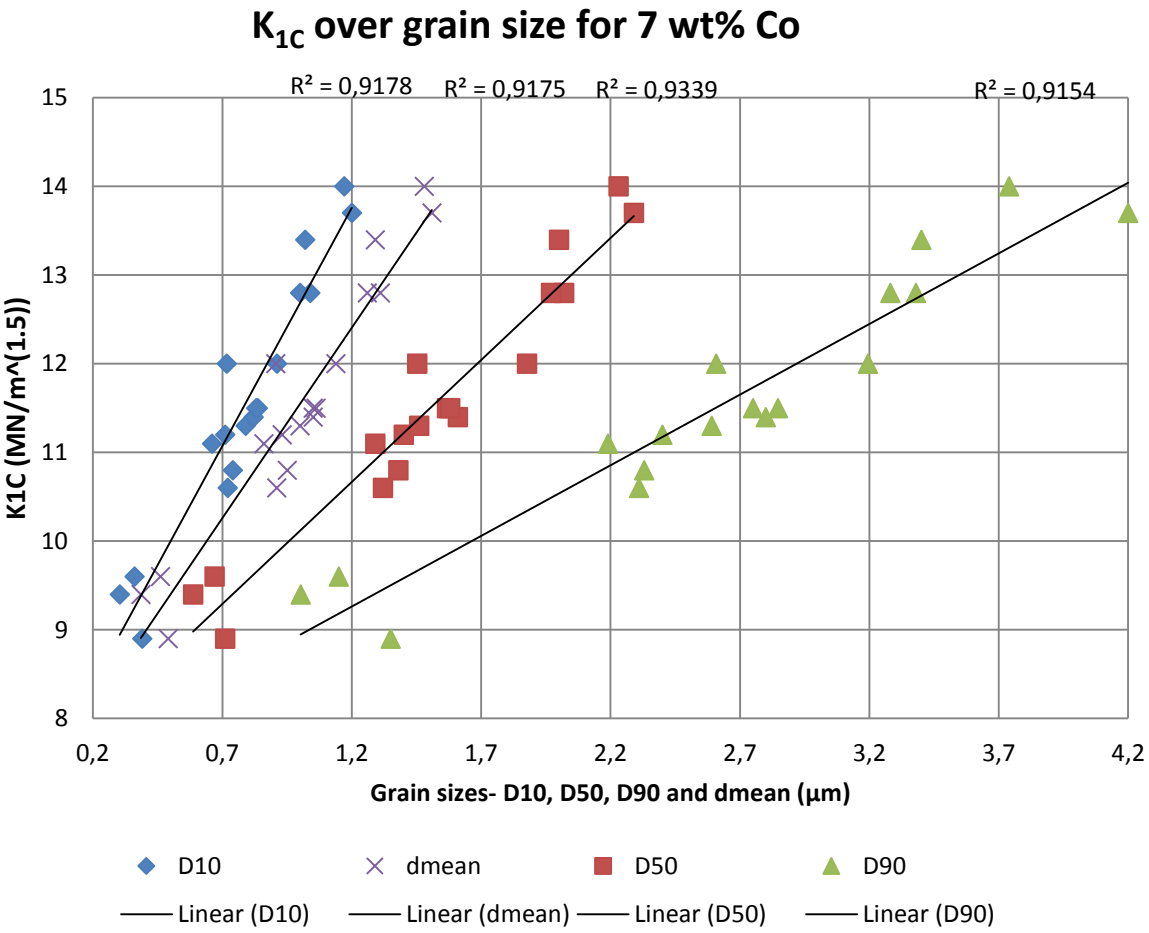

Figure 16, Fracture toughness (K1C) plotted against the grain size measured as D10, D50, D90 and dmean with linear trend lines and coefficients of determination (R^2) displayed for each data set, for cemented carbides with 7% Co.

Figure 17 shows how the dependence of fracture toughness to grain size (D50) changes with composition. Variations in Cobalt content influences fracture toughness greatly and K_{1C} is significantly larger for cemented carbides with 13% Co compared to 7%Co for similar grain sizes. However no significant change in fracture toughness is noted for cemented carbides of similar grain sizes with and without Cr-addition.

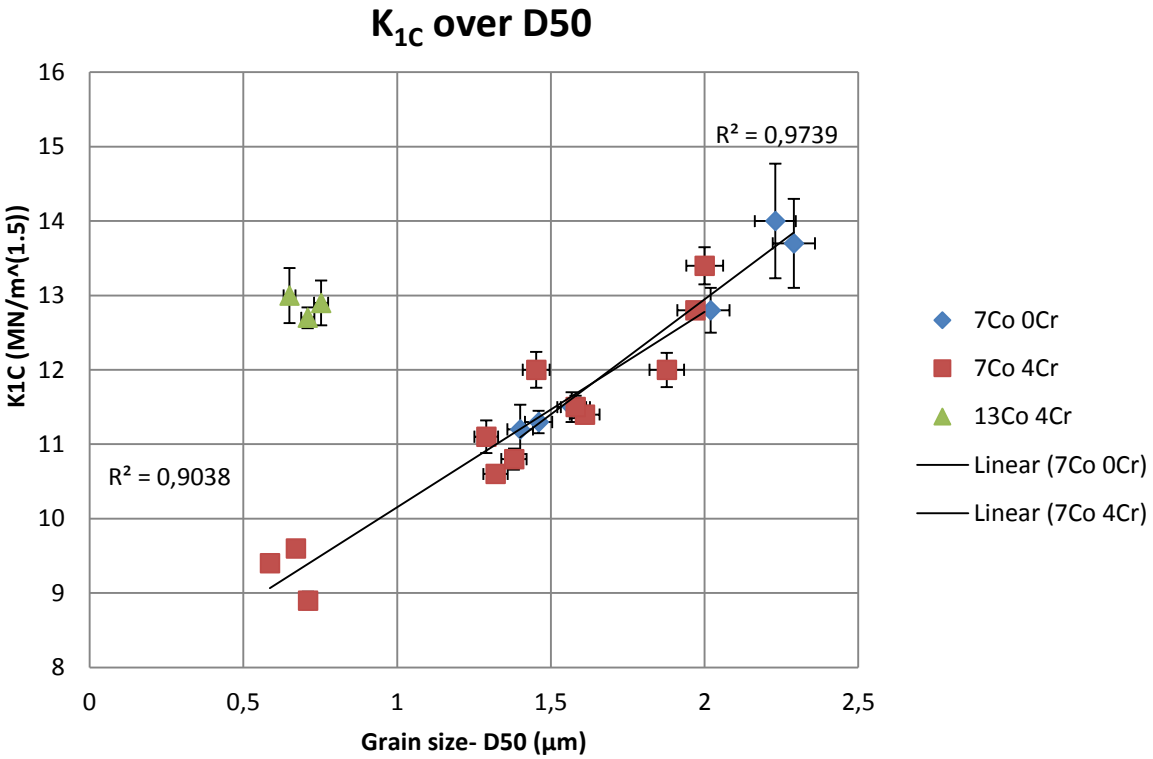

Figure 17, Fracture toughness (K1C) plotted against the grain size measured as D50 for cemented carbides with: 7%Co 0Cr (blue), 7%Co 4Cr (red) and 13%Co 4Cr (green) with linear trend lines and coefficients of determination (R^2) displayed for cemented carbides with 7% Co.

Coercivity and toughness

From the linear dependence of coercivity (Hc) to reciprocal grain size and fracture toughness (K1C) to grain size one can show that the fracture toughness (K1C) should be proportional to coercivity according to:

$$K_{1C} \propto \frac{1}{Hc - K}$$

Where K is the constant where the linear dependence of coercivity to the inverse grain size intercepts the y-axis (i.e. the coercivity for the bizarre case where WC - grain size goes to infinity for a 7% Co cemented carbide). Figure 18 shows such a linear relation where K=5.5. The vertical error bars shown in Figure 18 represents the standard deviation for each measurement, whilst the horizontal error bars represent a relative uncertainty of 2.5% (consistent with uncertainties of ±0.05 kA/M for coercivity measurements and ±0.1 kA/m for the constant K).

Figure 18 shows fracture toughness (K1C) plotted against 1/(Hc-5.5) and a linear trend line with a coefficient of determination R^2=0.926.

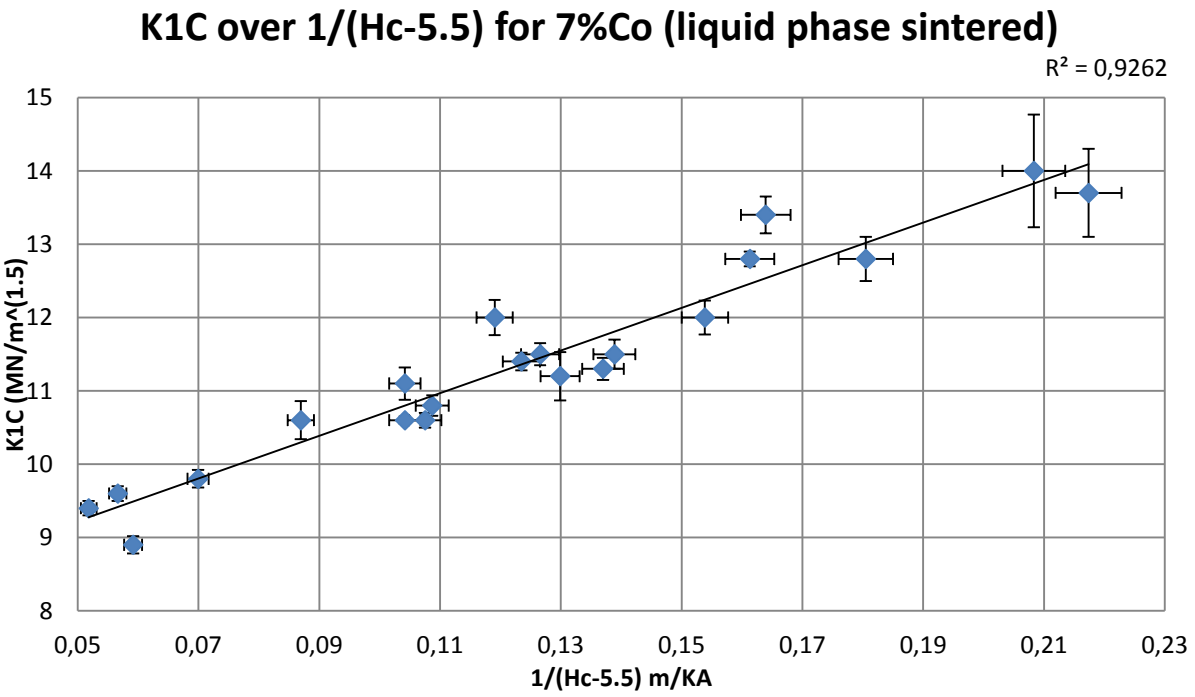

Figure 18, Fracture toughness (K1C) plotted against 1/(Hc-5.5) for cemented carbides with 7% Co and liquid phase sintered (i.e. to 1380˚C for 30min, 1430˚C for 1h and 1430˚C for 2h) with linear trend line and coefficient of determination (R^2) displayed on the chart.

Coercivity and hardness

Similar to the argument for coercivity and toughness above it can be argued that from the linear dependence of coercivity (Hc) to reciprocal grain size and hardness to the inverse square root of grain size one can show that the hardness H should be proportional to coercivity according to:

$$H \propto \sqrt{Hc - K}$$

Where K is the constant where the linear dependence of coercivity to the inverse grain size intercepts the y-axis. Figure 19 shows plot of the hardness as a function of $\sqrt{Hc - K}$ where K=5. 5. The vertical error bars shown in Figure 19 represents the standard deviation for each measurement, whilst the horizontal error bars represent a relative uncertainty of 2,5% (consistent with uncertainties of ±0.05 kA/M for coercivity measurements and ±0.1 kA/m for the constant K).

Figure 19 shows Hardness plotted against square root of (Hc-5.5) and a linear trend line with a coefficient of determination R^2=0.979.

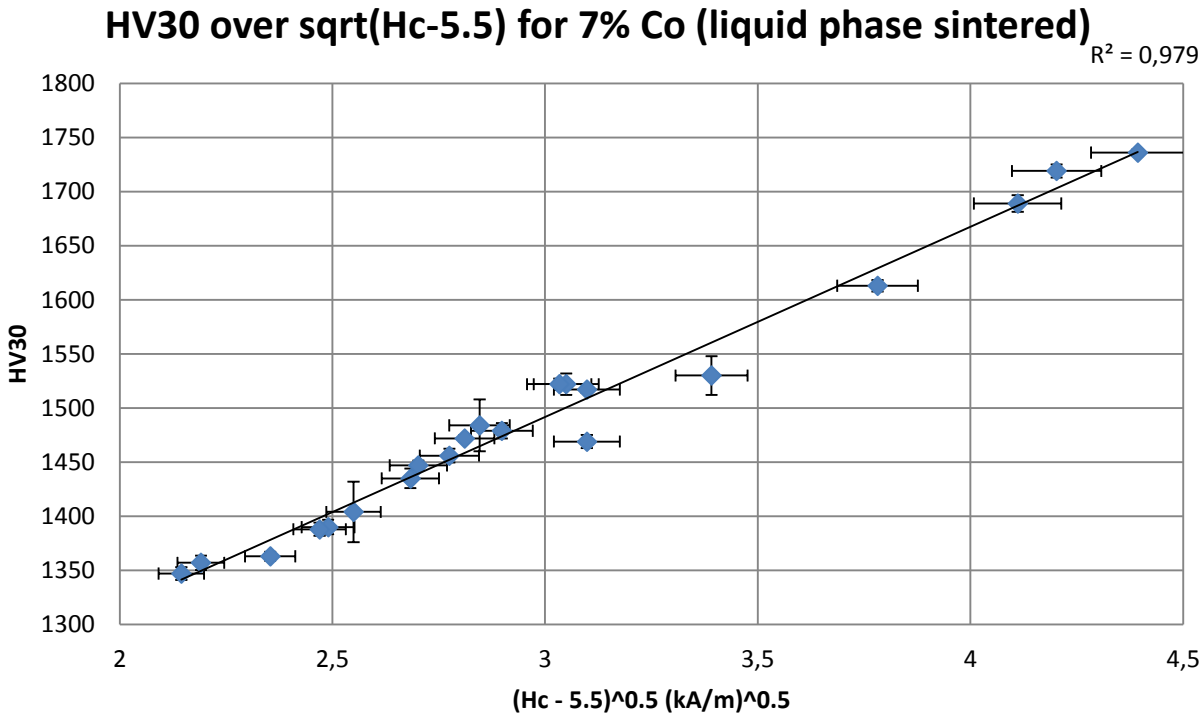

Figure 19, Hardness plotted against the square root of (Hc-5.5) for cemented carbides with 7% Co after liquid phase sintering (i.e. to 1380˚C for 30min, 1430˚C for 1h and 1430˚C for 2h) with linear trend line and coefficient of determination (R^2) displayed on the chart.

Toughness and hardness

Figure 20 shows fracture toughness as a function of hardness with standard deviations of the measurements shown as error bars. For cemented carbides with similar fracture toughness those with Cr- additions appear to be slightly harder. It is also noted that increased Co content gives a higher toughness/hardness ratio to the cemented carbides.

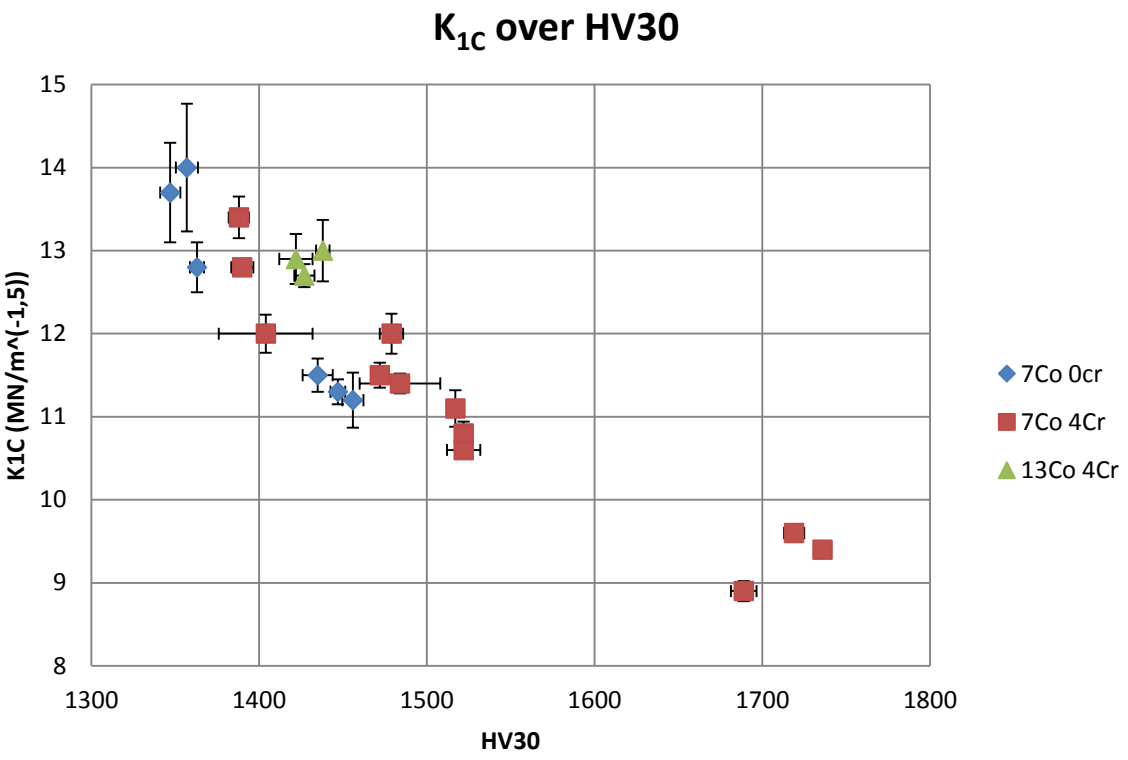

Figure 20, K1C plotted against HV30 for cemented carbides with: 7%Co 0Cr (blue), 7%Co 4Cr (red) and 13%Co 4Cr. Error bars show standard deviations from the measurements.

Discussion

Laser diffraction vs. electron backscatter diffraction

GSD as measured on the powder after milling with LD has a different shape than the GSD measured with EBSD for samples sintered at 1200˚C for 30min, where the sintered samples have a narrower GSD, see Figure 6. This implies that either grain growth has occurred for the samples sintered at 1200˚C for 30min or that there are discrepancies in either analysis method which makes GSDs measured with LD and EBSD incompatible for comparison.

Sample preparations are very different for the two analysis methods and segregation of grains could be a cause for error. In LD analysis the powder of homogenous granules was dissolved with hydrochloric acid to free the individual WC grains. Samples were then centrifuged and the clear supernatant was removed with a pipette. As this was done it is possible that some WC grains were removed with the supernatant. This was minimized by pipetting straight after the sample came out of the centrifuge and by avoiding agitation at this stage. It is more likely that smaller grains were removed with the supernatant and this would distort the distribution left in the sample. After removing the supernatant the sample was suspended in water co-block polymer solution. It is more likely that smaller grains remain in suspension whilst larger grains might sink to the bottom. Even though the solution was agitated with ultrasound during sampling and sample was taken from the middle of the test tube to avoid segregation it is possible that the sample had an unrepresentative size distribution. This would distort the GSD and such segregation could also explain the large variations observed for LD measurements, see Table 6. LD measurements also had relatively large background which was minimized by cleaning the glass in the sample chamber. However the background could be cause for uncertainties in the measurements. The background noise was relatively larger for the detectors responsible for measuring large particles, but smaller particles scatter light at lower intensities, so it is hard to say which part of the distribution was more affected by the background noise. For EBSD analysis an area is selected in a cross-section of the sintered sample. Before sintering the powder with homogenous granules were pressed together and it is less likely for the grains to segregate during the sintering process. Segregation in sampling for LD analysis could perhaps account for the different GSDs obtained through LD and EBSD analysis as the finer grains might be over represented. However it is also possible that small grains are removed with the supernatant while large grains are not suspended, hence the distribution could be even wider than what was measured.

For quantitative comparison between LD and EBSD measurements it would be necessary to have EBSD analysis of samples where no grain growth has occurred for them to be reliable. It would be reasonable then that LD measurements result in larger grain sizes but with similar shape of the distribution since EBSD measures a cross section, i.e. in 2D. As can be seen in Figure 6, the D50 value measured with LD for raw material C is similar to the D50 measured with EBSD for cemented carbide 6 (C 7Co 4Cr). This indicates that grain growth had occurred for cc-6 already when sintered to 1200˚C for 30 min. However, for similar comparison between LD measurements of raw material A and cc- 1 (A 7Co 4Cr) in Figure 6, larger grain sizes are seen for the raw material, as would be expected. This would indicate that cc-1 has not undergone as much grain growth as cc-6 when sintered to 1200˚C for 30min. However, this not plausible since both cc-1 and 6 have the same composition in regard to Co and Cr and smaller grains have larger driving force for grain growth. Thus it is unreasonable to make any qualified comparisons between the two methods without further information.

Shrinkage/densification

Linear shrinkage for reaching full density was similar for all cemented carbides except 3 and 4, containing raw material B1, these cemented carbides shrunk more before reaching full density, see Table 8. This indicates that raw material B1 exhibits less compaction during pressing.

The results from Table 8 indicate that Cr additions decrease the densification in solid state sintered bodies, consistent with results from Bounhore et al. [25] who studied 'The effect of Cr-additions on solid state sintering of WC-Co alloys'. They argue that surface Cr oxides interfere with wetting of WC grains by Co, by delaying the dispersion of Co at the beginning of densification. They found that the onset of densification started at 1000-1100˚C for Cr-doped alloys, consistent with the reduction temperature of Cr-oxides. Results from Table 8 also indicate that for cemented carbides with smaller average grain sizes reached higher densities when sintered to 1200˚C for 30min and 1300˚C for 10min, when comparing samples with Cr-additions. This is likely due to a higher mobility for the smaller grains and a larger driving force for grain growth.

Grain Growth

The grain growth observed in Figures 7-10 can be divided in three stages: an initial rapid grain growth during solid state sintering where grain growth of the fine fraction are more prominent (Figure 7); a secondary stage of slower grain growth during liquid phase sintering and a third stage where the onset of abnormal grain growth after longer sintering is observed as the growth of larger grains grow out of proportion to the rest of the population (Figures 9 and 10).

The first stage where growth of the fine fraction is more pronounced is consistent with solution of finer WC grains in the Co binder as a mechanism of grain growth but also with the theory of grain growth through coalescence, as smaller grains require less energy to rotate and coalesce. From Figure 7 it can be seen that growth of D10 is affected by Cr-additions and Co variations mainly at this first stage since: The D10 value for cc 7 and 4 (no Cr) grows larger than for cc 6 and 3 (with Cr) respectively, the biggest differences seen between 2000-10 000 K*min. For higher sintering effects D10 values grow at similar rates with or without Cr additions. The same can be said comparing D10 for cc 1 (7Co) and 2 (13Co).Furthermore the prominent growth of finer grains at the initial stage accounts for a narrower GSD as observed when comparing LD to EBSD measurements (Figure 6).

The secondary stage where the grain growth slows down affects the entire GSD: The growth of D10 slows down but continues throughout the sintering process for all cemented carbides investigated, see Figure 7. The growth of D50 value is slowed almost to a halt for cemented carbides with Cr-additions whilst D50 for cemented carbides without Cr continues to grow throughout the sintering process, see Figure 8. The growth of D90 and D95 is also slowed down almost to a halt for cemented carbides with Cr-additions while those without Cr grow steadily until the third stage is initiated, see Figures 9 and 10.

The third stage, where larger grains grow out of proportion, is consistent with abnormal growth with 2D-nucleation as the rate controlling step. This stage can only be seen for cemented carbides without Cr at the later sintering stages, see D90 and D95 for cc 6 and 3 (no Cr) in Figure 9 and 10.Cr-additions thus seem to prevent the onset of abnormal grain growth for the cemented carbide grades at the sintering conditions investigated and decrease the growth rate during the liquid phase sintering.

The Cr-additions have most impact in the D10 at the first stage, affects the D50 during the entire sintering period but especially has an impact on D90 and D95 at the later sintering stages. It can be argued that the inhibition mechanisms of Cr additions are related to the precipitation rather than dissolution of grains for growth by solution and precipitation. This could happen via various mechanisms, such as formation of stable clusters with the W and C atoms dissolved in the binder or at the interface where Cr is found at larger proportions than in the bulk Co [5]. It is however seen from Figure 7 that Cr additions also have an impact on the D10 value at early sintering stages, where the growth of D10 should be governed by the dissolution of fine grains. However growth by solution and precipitation is a dynamic process and a fraction of the smaller grain are bound to grow by precipitation. Thus inhibition of precipitation would explain why the Cr additions also affect the D10 value in the early stage of sintering.

Figure 10 shows similar trends for the D95 value as Figure 9 did for the D90 value. The increase in growth rate of D95 for cemented carbides without Cr-additions at the later sintering stage seen in Figure 10 is however more marked than what could be seen for D90 in figure 9. Therefore it is perhaps more helpful to look at the D95 value for identification of an onset of abnormal grain growth. However, a decrease in D95 is noted for cemented carbides 3 and 5 at the later sintering stage, which illustrates that the D95 value is not as statistically reliable as D90. This is understandable since D95 represents only a small fraction of the grains in the population and better statistics would be needed to get a reliable value for D95.

Uncertainties of 3% indicated by the error bars in Figures 7-10 seem reasonable for these analyses. The D50, D90 and D95 values decrease for cemented carbide 5 at the later sintering stage. This is most likely an artefact of the uncertainties in these measurements. 3% error seems to cover this discrepancy.

Cr and grain growth in the solid state

After sintering at 1200˚ for 30min a difference can be observed in grain size between cemented carbides 6 (C 7Co 4Cr) and 7 (C 7Co 0Cr), where cc- 7 exhibits larger grains. The difference being most prominent for the D10, where D10 for cc-7 is 12% larger than D10 for cc-6, see Table 7. This indicates that the delayed onset of densification due to the presence of surface Cr-oxides also delays the onset of grain growth. This is reasonable since the grain growth is facilitated as the WC grains are wetted with Co [6].However after sintering to 1300˚C for 10min similar grain sizes can be observed for cc 6 and 7, which indicate that the delayed onset of densification has little effect on the grain growth as sintering proceeds. Cr-additions are known to decrease the melting temperature of cobalt in the system, see Figure1. This could explain why D10 is similar for cc- 6 and 7 after sintering to 1300˚C for 10min.The D10 for cemented carbides 3 (B1 7Co 4Cr) and 4 (B1 7Co 0Cr) differ with 6% at 1300˚C 10min (Table 7) which indicate that Cr affects grain growth at solid state more for smaller grain sizes.

7 and 13% Co

Variations in the amount of Co binder between 7 and 13% for raw material A had small effects on grain growth. D10 and D50 values were relatively higher for cemented carbide 2 (A 13Co 4Cr) compared to 1 (A 7Co 4Cr), see Figures 7 and 8. D90 and D95 were more similar, see Figures 9 and 10. This indicates a more pronounced grain growth for the fine fraction of grains at larger Co contents than for the larger grains. This is most likely due to increased dissolution of the smaller grains for an increased amount of Co. It is notable that the D90 and D95 with 7%Co seems to surpass

the D90 and D95 with 13%Co after sintering to 1430˚C for 2h (Figure 9 and 10), this is however thought to be within the margin of error and further interpretations of this are deemed unreliable.

The differences between 7 and 13%Co seen in Figure 7 and 8 were more pronounced at the initial sintering stage. This is also consistent with the dissolution of grain in the Co binder. Grain growth being similar for the larger grains is probably due to the presence of Cr as a grain growth inhibitor, since Cr-additions seem to affect the precipitation, and greater differences might be seen if the grains are allowed to grow abnormally, i.e. without grain growth inhibitor, for longer sintering cycles. No samples with 13% Co were prepared without Cr-additions in this project and further analysis of how the increase in Co content affects grain growth is left for future work.

Variations in CMA and coalescence

The appearance of variations in GSD measured when using a 1˚ or 5˚ critical misorientation angle for grain determination can be explained by coalescence. The gradual disappearance of variations in GSD when using a 1˚ or 5˚ CMA for samples as they are further sintered (see Table 9) indicates the alignment of grains with a misorientation angle< 5˚. The fact that smaller variations in GSD were observed for cemented carbides with smaller average grain size would then indicate that such an alignment had already occurred, as the smaller grains require less energy to align. The fact that the variations are observed for the fine fraction of grains in materials with large average grain size is also consistent with coalescence as these grains are more likely to coalesce.

However it is also possible that the observed variations in GSD measured are due to deformations in the WC- grains, where 1˚ CMA would identify deformations in a grain as false grains. The occurrence of the observed variations in GSD increasing for grades with larger average grain size would then be explained by more energy required for the annealing of such deformations. The identification of deformations as false grains is likely to appear odd in the EBSD map, with grains inside larger grains as an artefact. No such oddities were found in the EBSD maps analyzed. However, the resolution of the map is not good enough to draw any conclusions about these individual grains and further investigations are advised.

Material properties

There was good coherence with known relations correlating hardness (Figure 12) and coercivity (Figure 14) to grain size for cemented carbides with 7% Co, sintered to full density. Also a linear relation was found between the fracture toughness and grain size for the same cemented carbides, see Figure 16. The D50 value gave the best fit for linear regressions of coercivity to reciprocal grain size (Figure 14), hardness to the inverse square root of grain size (Figure 12) and fracture toughness to grain size (Figure16). This is reasonable since D50 gives the best representation for the grain size for a Gaussian distribution. Previous results by Persson and Schwind [19] have indicated a better fit for the D10 value for the linear relation between coercivity and reciprocal grain size; this was however for GSDs that were deliberately skewed. The coercivity gave a higher coefficient of determination for linear regression to reciprocal grain size than hardness did to the inverse square root of grain size and fracture toughness to the grain size (Figures 12, 14 and 16). Presumably coercivity gives better fit for linear regression due to smaller uncertainties of measurements than hardness and fracture toughness. Standard deviations from measurements of hardness and fracture toughness displayed in the results might overestimate the reliability of the methods, especially across operators where larger uncertainties are expected. However, all values measured and

displayed in this thesis were performed by the same operator (the author), which makes for more reliable comparison between results.

No significant effect of Cr-additions to trends for fracture toughness (Figure 17) to grain size or coercivity (Figure 15) to reciprocal grain size were observed for cemented carbides sintered to full density. Hardness values seemed to increase slightly for cemented carbides with Cr additions (Figure 13). This is interesting since the volume fraction binder phase increases with the Cr additions, as Cr dissolves in the binder phase. From Figure 15 it was observed that solid state sintered cemented carbides deviate from the otherwise linear trend between coercivity and reciprocal grain size. These cemented carbides exhibited lower coercivity than expected from the trend. This indicates that the cobalt domains are larger than expected consistent with a delayed dispersion of Co in the solid state.

Since there were good correlations for coercivity, hardness and fracture toughness to grain size it is reasonable to make relations between coercivity and toughness (Figure 18) as well as between coercivity and hardness (Figure 19). This was done and data made for good fit with linear regression. Hardness gave a better coefficient of determination than fracture toughness, which is reasonable since fracture toughness is calculated using hardness values and crack lengths, which makes inherent uncertainties higher. Relations for coercivity to hardness and fracture toughness provide reasonable estimates of mechanical properties from a non-destructive analysis method. They are however limited to cemented carbides with 7%Co, carbon content corresponding to the middle of the two phase window and a Gaussian size distribution. Extrapolations outside the ranges investigated here should be done with caution.

The variations between GSDs for the different sintering cycles might affect the material properties. However, the uncertainties in measurements of hardness and toughness are too large to draw any relevant conclusions between the shape of the GSD and hardness/fracture toughness for the variations in GSD observed in this thesis project. The D50 value gave good fit to linear regressions and is deemed representative of the GSD.

Sintering times investigated were never longer than 2h and what is described as an onset of abnormal grain growth above does not seem to affect the GSD to an extent where this significantly affects the mechanical properties of the material. Further sintering where the abnormal growth is allowed to proceed should however affect the material properties in a detrimental manner.

Conclusion

The conclusion from comparison between LD and EBSD measurements is that a quantitative comparison for samples sintered at 1200˚C for 30min is inconclusive. It is however likely that some grain growth has occurred already for sintering at 1200˚C for 30min which would explain narrowing of the GSD.

The observed grain growth can be divided in three stages for the sintering conditions investigated:

- Initial rapid grain growth during solid state sintering where grain growth of the fine fraction is more prominent.
- A secondary stage of slower grain growth during liquid phase sintering
- A third stage where the onset of abnormal grain growth after longer sintering is observed as the growth of larger grains grow out of proportion to the rest of the population

The presence of Cr-additions delay the onset of the initial stage, decrease the growth rate for the second stage and prevents the third stage. Most likely the delay of the initial stage is related to the presence of Cr- surface oxides which delay the spreading of Co at the beginning of densification whilst the inhibition at the secondary and tertiary stages is likely related to an inhibited precipitation of W and C atoms dissolved in the Co binder onto existing WC grains.

The effect of variations between 7 and 13% Co were small, presumably due to inhibition of grain growth by Cr-additions.

Results found by varying the CMA for the determination of grains after EBSD analysis is consistent with coalescence, where bordering grains with a misorientation angle <5˚ coalesce during sintering. The reliability of such interpretations should however be further investigated.

Relations between coercivity and hardness/toughness for cemented carbides with 7%Co and similar carbon content gave good fit for linear regression, and can be used as an estimate for hardness and toughness for such cemented carbides. It is however stressed that these interpretations are most likely limited to cemented carbides with a lognormal size distribution, within the variations observed in this project.

Future work

Further investigations for comparison between LD and EBSD measurements are needed to compare the results between the different methods. EBSD measurements of a cross-section on the powder are suggested, where a cross section could be polished on powder set in epoxy using a cross-section ion polisher.

Further, to be able to draw a conclusion on whether the variations in CMA can be reliably interpreted as coalescence further investigation is required. Identification of coalescence as a mechanism for grain growth by EBSD analysis could be an interesting venue to investigate further, investigating to what stage coalescence is a relevant growth mechanism and perhaps to draw conclusions on the mobility of grains of different sizes in the cemented carbides. It might be due to other factors but misorientation angles between grains below 5˚ gradually disappear as sintering goes along.

Also the relations found between coercivity and hardness /toughness can be expanded to include variations in Co binder content. Samples with 13%Co should be prepared without Cr additions to better understand how the increase in binder content affects grain growth.

References

1 - Uhrenius, B 2000, Pulvermetallurgi, Stockholm: Institutionen för materialvetenskap, Kungl. Tekniska högsk., 2000, (2001).

2 – Hellsing, M, High resolution microanalysis of binder phase in as sintered WC-Co cemented carbides, Materials Science and Technology, 4 (1988)824

3 – Haglund, S, and Ågren, J 1998, W content in Co binder during sintering of WC-Co, Acta Mater., 46, (2801-7).

4 - Borgh, I, Hedström, P, Persson, T, Norgren, S, Borgenstam, A, Ågren, J, & Odqvist, J 2014, 'Microstructure, grain size distribution and grain shape in WC–Co alloys sintered at different carbon activities', International Journal of Refractory Metals and Hard Materials, vol. 43, pp. 205-211.

5 - Johansson, S 2010, A computational study of interface structures and energetics in cemented carbides and steels, Göteborg: Chalmers University of Technology, 2010.

6 - Wang, X, Fang, ZZ, & Sohn, HY 2008, 'Grain growth during the early stage of sintering of nanosized WC–Co powder', International Journal of Refractory Metals and Hard Materials, vol. 26, pp. 232-241.

7 - Zhong, Y, & Shaw, LL 2011, 'Growth mechanisms of WC in WC–5.75wt% Co', Ceramics International, vol. 37, pp. 3591-3597.

8 - Borgh, I 2013, Aspects of structural evolution in cemented carbide: carbide size, shape and stability, Stockholm: Industrial Engineering and Management, KTH Royal Institute of Technology, 2013

9 - Park, Y, Hwang, N, & Yoon, D 1996, 'Abnormal growth of faceted (WC) grains in a (Co) liquid matrix', Metallurgical and Materials Transactions A, vol. 27, no. 9, p. 2809.

10 – W.D. Schubert 2012 'WC Grain Growth Inhibition in Hardmetals Looking Back 30 Years of R&D at Vienna University of Technology' Zhuzhou International Conference on Cemented Carbides pp. 058-079

11 - Mannesson, K, Jeppsson, J, Borgenstam, A, & Ågren, J 2011, 'Carbide grain growth in cemented carbides', Acta Materialia, vol. 59, pp. 1912-1923.

12 - Mannesson, K, Borgh, I, Borgenstam, A, & Ågren, J 2011, 'Abnormal grain growth in cemented carbides — Experiments and simulations', International Journal of Refractory Metals and Hard Materials, 29, pp. 488-494

13 - Engqvist, H, & Uhrenius, B 2003, 'Determination of the average grain size of cemented carbides', International Journal of Refractory Metals & Hard Materials, vol. 21, no. 1/2, p. 31.

14 - Jeppsson, J, Mannesson, K, Borgenstam, A, & Ågren, J 2011, 'Inverse Saltykov analysis for particle-size distributions and their time evolution', Acta Materialia, vol. 59, pp. 874-882. Available from: 10.1016/j.actamat.2010.09.046

15 - Borgh, I, Hedström, P, Odqvist, J, Borgenstam, A, Ågren, J, Gholinia, A, Winiarski, B, Withers, P, Thompson, G, Mingard, K, & Gee, M 2013, 'On the three-dimensional structure of WC grains in cemented carbides', Acta Materialia, 61, pp. 4726-4733,

16 - J Freitag, P Walter and HE Exner, Charakterisierung der Binderphase von WC-Co Hartmetallen über magnetische Eigenschaften, Z Metallkd, 69 (1978) 546-9

17 -B. Jansson, J. Qvick, Proceedings of the 16th International Plansee Seminar, vol. 2, Reutte, Austria (2005), pp. 1197–1206

18 - Roebuck, B 1995, 'Terminology, testing, properties, imaging and models for fine grained hardmetals', International Journal of Refractory Metals and Hard Materials, vol. 13, no. Special Issue on Fine Grained Hardmetals, pp. 265-279

19 – T. Persson, M. Schwind, Proceedings of the 18th international Plansee Seminar, Reutte, Austria (2013) HM98

20 - Shetty, DK, Wright, IG, Mincer, PN, & Clauer, AH 1985, 'Indentation fracture of WC-Co cermets', Journal of Materials Science, vol. 20, no. 5, p. 1873.

21 -Sheikh, S, M'Saoubi, R, Flasar, P, Schwind, M, Persson, T, Yang, J, & Llanes, L 2015, 'Fracture toughness of cemented carbides: Testing method and microstructural effects', International Journal of Refractory Metals and Hard Materials, vol. 49, no. Special Issue: International Conference on the Science of Hard Materials - 10, pp. 153-160

22 - Williams, DB, & Carter, CB 2009, Transmission Electron Microscopy. A Textbook for Materials Science, Boston, MA: Springer US, 2009

23 - Schwartz, AJ, Kumar, M, Adams, BL, & Field, DP 2009, Electron Backscatter Diffraction in Materials Science, Boston, MA : Springer US, 2009.

24 - http://www.malvern.com/ (2015-11-20)

25 - Bounhoure, V, Lay, S, Coindeau, S, Norgren, S, Pauty, E, & Missiaen, J 2015, 'Effect of Cr addition on solid state sintering of WC–Co alloys', International Journal of Refractory Metals and Hard Materials, vol. 52, pp. 21-28.